Learning Cocoercive Conservative Denoisers via Helmholtz Decomposition for Poisson Imaging Inverse Problems

Deliang Wei

School of Mathematical Sciences, East China Normal University, Shanghai 200241, China 52215500006@stu.ecnu.edu.cn

Haobo Xu

School of Mathematical Sciences, East China Normal University, Shanghai 200241, China 52275500009@stu.ecnu.edu.cn

Fang Li*

School of Mathematical Sciences, Key Laboratory of MEA (Ministry of Education), Shanghai Key Laboratory of PMMP, East China Normal University, Shanghai 200241, China fli@math.ecnu.edu.cn

Peng Chen

School of Mathematical Sciences, East China Normal University, Shanghai 200241, China 52265500005@stu.ecnu.edu.cn

Jiale Yao

School of Mathematical Sciences, East China Normal University, Shanghai 200241, China 52285500019@stu.ecnu.edu.cn

Tievong Zeng

Institute for Advanced Study,
Beijing Normal-Hong Kong Baptist University,
Zhuhai 519000, Guangdong, China
School of Mathematics and Statistics,
Guangzhou Nanfang College,
Guangzhou 510970, Guangdong Province, China
tieyongzeng@uic.edu.cn

Abstract

Plug-and-play (PnP) methods with deep denoisers have shown impressive results in imaging problems. They typically require strong convexity or smoothness of the fidelity term and a (residual) non-expansive denoiser for convergence. These assumptions, however, are violated in Poisson inverse problems, and non-expansiveness can hinder denoising performance. To address these challenges, we propose a cocoercive conservative (CoCo) denoiser, which may be (residual) expansive, leading to improved denoising performance. By leveraging the generalized Helmholtz decomposition, we introduce a novel training strategy that combines Hamiltonian regularization to promote conservativeness and spectral regularization to encourage cocoerciveness. We prove that CoCo denoiser is a proximal operator of a weakly convex function, enabling a restoration model with an implicit weakly convex prior. The global convergence of PnP methods to a stationary point of this restoration model is established. Extensive experimental results demonstrate that our approach outperforms closely related methods in both visual quality and quantitative metrics. A test code is provided for reproducibility².

^{*}Corresponding author

²https://github.com/FizzzFizzz/CoCo-PnP

1 Introduction

Image restoration is a fundamental task in the computer vision field. Although most works assume that the noise follows Gaussian distribution [43, 12], under low-light condition, such as hyperspectral imaging [53, 17], medical imaging [67], and limited photon imaging [13], images are inevitably corrupted by Poisson noises. In this paper, we focus on solving Poisson inverse problems by Plug-and-Play (PnP) methods.

The following formula describes the Poisson corruption procedure:

$$f \sim \text{Poisson}(pKu)/p,$$
 (1)

where u is the potential image, f is the noisy image, the peak value p is the average number of photons recieved per pixel, and K is a known linear operator such as identity I, blur kernel, or Radon transform. A small p corresponds to a severe noise environment. In order to recover u from f, a variational approach is considered:

$$\arg\min_{u \in V} F(u) + G(u), G(u) = \lambda \langle \mathbf{1}, Ku - f \log Ku \rangle, \tag{2}$$

where V is the underlying Hilbert space endowed with the inner product $\langle \cdot, \cdot \rangle$, F denotes the prior regularization term, and the data fidelity G is the Bregman divergence, with $\lambda > 0$ being the balancing parameter. Typical choices for F includes total variation [59] and its variants [33, 11], weighted nuclear norm [23], and group-based low rank prior [44]. First order methods are employed to find \hat{u} , such as the proximal gradient descent method (PGD):

$$u^{k+1} = \text{Prox}_{\frac{F}{2}}(u^k - \beta^{-1}\nabla G(u^k)),$$
 (3)

and the alternating direction method with multipliers (ADMM) [10]:

$$u^{k+1} = \operatorname{Prox}_{\frac{F}{\beta}}(v^k - b^k), v^{k+1} = \operatorname{Prox}_{\frac{G}{\beta}}(u^{k+1} + b^k), b^{k+1} = b^k + u^{k+1} - v^{k+1},$$
(4)

where $\beta>0$ is a balancing parameter. For a closed, convex and proper (CCP) function $F:V\to \bar{\mathbb{R}}=(-\infty,\infty]$, the proximal operator $\operatorname{Prox}_F:V\to V$ is defined as: $\operatorname{Prox}_F(y):=\arg\min_{x\in V}F(x)+\frac{1}{2}\|x-y\|^2$.

Plug-and-play methods. By replacing $\operatorname{Prox}_{\frac{F}{\beta}}(\cdot)$ with an off-the-shelf Gaussian denoiser $\operatorname{D}_{\sigma}(\cdot)$, where σ denotes the denoising strength, Venkatakrishnan et al. introduced the plug-and-play ADMM (PnP-ADMM) algorithm [69]. Since then, PnP methods have achieved surprisingly remarkable recovery results in many inverse problems, including bright field electron tomography [64], diffraction tomography [65], camera image processing [25], low-dose CT imaging [9, 72], Poisson image denoising [38, 27], deblurring [36], inpainting [77], and super-resolution [37, 32].

Challenges. Despite the impressive recovery performance, the convergence analysis of PnP methods remains challenging, especially in the context of Poisson inverse problems. The standard convergence of ADMM and PGD relies on the convexity of both F and G. However, a convex prior term F often leads to limited recovery performance. When F is weakly convex, additional assumptions on G, such as strong convexity or smoothness, are required. Unfortunately, these assumptions do not hold in Poisson inverse problems. Moreover, in general, a deep denoiser is not a proximal operator, which further complicates the situation.

In order to get a proximal D_{σ} , it should satisfy some Lipschitz properties such as non-expansiveness, and be the (sub)gradient of some CCP potential ϕ [47, 22]. In the following, we briefly discuss approaches to satisfy these conditions, as well as some related convergent PnP methods.

Lipschitz property. There are mainly two methods to ensure the Lipschitz property: **real spectral normalization (RealSN)** and **spectral regularization (SR)**. Ryu et al. enforced a contractive $I - D_{\sigma}$ by applying RealSN to the denoiser, which normalized the spectral norm of each layer [60]. However, RealSN is computationally expensive, and was specifically designed for denoisers with cascade residual learning structures, such as DnCNN [74], making it unsuitable for other networks like UNet [58]. A more flexible approach is SR technique introduced by Terris et al. [66]. In order to get a firmly non-expansive D_{σ} , they added a spectral term $\min\{1 - \epsilon, \|2J - I\|_*\}$ to the original loss

function, such that $\|2\,J-I\|_* \le 1$, where $J = \nabla\,D_\sigma$ is the Jacobian matrix of D_σ , and $\epsilon \in (0,1)$ is a pre-defined parameter. With this spectral constraint, D_σ is firmly non-expansive, and thus becomes the resolvent of some implicitly maximally monotone operator (RMMO), incorporated into the Douglas-Rachford splitting (DRS) method. RMMO-DRS only requires a convex fidelity, making it suitable for Poisson inverse problems. Inspired by SR, Wei et al. proposed to train a strictly pseudo-contractive (SPC) denoiser, termed SPC-DRUNet [71]. By incorporating the Ishikawa process and half-quadratic splitting (HQS), they developed the PnPI-HQS method. The convergence of PnPI-HQS only requires a convex fidelity term G, which makes it suitable for Poisson problems. SPC is much weaker than firm or residual non-expansiveness. However, SPC-DRUNet is in general not a proximal operator, and PnPI-HQS does not solve any optimization problem.

Conservativeness. To ensure the conservative property, many works attempt to explicitly define a prior function ϕ , such that the denoiser is its gradient or proximal operator. Romano et al. proposed the regularization by denoising (RED) [57]. The RED prior term takes the form of $\phi(x) = \frac{1}{2}\langle x, x - z \rangle$ $D_{\sigma}(x)$. Under the assumptions that D_{σ} is locally homogeneous, and that ∇D_{σ} is symmetric with spectral radius less than one, Romano et al. proved that $D_{\sigma} = I - \nabla \phi$. Yet the assumptions might be impractical for deep denoisers as reported by Reehorst & Schniter [54]. Instead of training a Gaussian denoiser D_{σ} , Cohen et al. [16] parameterized ϕ with a neural network, $D_{\sigma} = \nabla \phi$. Unfortunately, as verified by Salimans & Ho [61], and Hurault et al. [28], directly modeling ϕ with a neural network leads to poor performance. To tackle this, Hurault et al. [28] introduced the gradient step (GS) denoiser, where $D_{\sigma} = \nabla \phi$, with $\phi(x) = \frac{1}{2} ||x||^2 - g_{\sigma}(x)$, $g_{\sigma}(x) = \frac{1}{2} ||x - N_{\sigma}(x)||^2$, where N_{σ} is a neural network. Then $D_{\sigma} = I - \nabla g_{\sigma} = N_{\sigma} + J_{N_{\sigma}}^{T}(I - N_{\sigma})$, where $J_{N_{\sigma}}$ is the Jacobian matrix of N_{σ} . N_{σ} uses the light DRUNet architecture [73], and such D_{σ} is called GS-DRUNet. Following this, they then proposed Prox-DRUNet, which trains a GS-DRUNet with a non-expansive residual $I - D_{\sigma}$ via SR [29]. They proved that Prox-DRUNet acts as a proximal operator of some weakly convex prior F. The Prox-DRS algorithm is given by plugging $L D_{\sigma} + (1 - L) I$ as the denoiser into DRS. Prox-DRS converges for proper closed fidelity G with $L \in [0, 0.5)$, making it applicable for Poisson inverse problems. However, this great work still requires a non-expansive residual, which alters the denoising performance, especially for large noises. To apply GS-DRUNet in Poisson inverse problems, Hurault et al. proposed to train a Bregman denoiser to remove Gamma noise [27]. Two convergent algorithms B-RED and B-PnP are derived. However, experimental results indicate that the Gamma denoiser struggles to remove large Gamma noise, thereby limiting the restoration performance.

Motivations. As discussed above, in order a get a proximal denoiser, it needs to be Lipschitz and conservative.

Typical Lipschitz conditions, such as non-expansiveness and residual non-expansiveness, are restrictive and lead to compromised performance. Weaker assumptions, like (strictly) pseudo-contractive conditions, can not guarantee a proximal denoiser. This limitation motivates us to explore a more suitable assumption that ensures the denoiser remains proximal while maintaining good denoising performance.

For the conservativeness, existing approaches typically construct an explicit potential function ϕ . While this idea is intuitively appealing and convenient for optimization, it raises a question: Is there any alternative approach to promote the conservativeness, without requiring an explicit prior, by directly regularizing the denoiser, without significantly changing its network structure?

Contributions. To address the issues outlined above, this paper introduces a novel training strategy for learning a proximal denoiser. Leveraging the SR technique and the generalized Helmholtz decomposition, we propose to train a cocoercive conservative (CoCo) denoiser. CoCo denoiser proves to be a proximal operator of some implicit non-convex prior function. Cocoerciveness is a weaker constraint on the denoiser, compared to existing constraints like firm or residual non-expansiveness. As a result, the CoCo denoiser not only achieves superior denoising performance but also enhances PnP recovery in Poisson inverse problems. Overall, our main contributions are fourfold:

- We introduce a novel assumption, cocoerciveness, for the deep denoisers. Cocoerciveness is strictly weaker assumption than non-epansive type assumptions, and therefore, less restrictive for denoisers.
- We shed a new light on the conservative assumption, by studying the denoising geometry. Using the generalized Helmholtz decomposition, a denoiser is implicitly decomposed into a conservative part and a Hamiltonian part. We show intuitively and rigorously that an ideal denoiser should be conservative with no Hamiltonian part.
- We prove that a CoCo denoiser is a proximal operator of some implicit prior. An effective training

strategy is proposed to promote these properties.

 A Poisson inverse model with an implicit prior is derived. The global convergence of PnP methods with CoCo denoisers is established.

2 CoCo denoisers

In this section, we propose CoCo denoisers. First, we introduce the cocoercive assumption, and its spectral distribution on the complex plane. Next, by the generalized Helmholtz decomposition, we show intuitively that an ideal denoiser should be conservative, with no Hamiltonian part. Then, we prove that a CoCo denoiser D_{σ} is the proximal operator of some weakly convex and smooth prior function $F:V\to \bar{\mathbb{R}}:=\mathbb{R}\cup\{\infty\}$, $D_{\sigma}=\operatorname{Prox}_{\frac{F}{\beta}}$. Finally, a restoration model with an implicit weakly convex prior is given.

2.1 Cocoercive denoisers

Let $V=\mathbb{R}^n$ be a real Hilbert space³ with inner product $\langle\cdot,\cdot\rangle$, and the induced norm $\|x\|=\sqrt{\langle x,x\rangle}$. Let $D:V\to V$ be an operator⁴. An operator $D:V\to V$ is said to be γ -cocoercive $(\gamma\in[0,\infty))$, if $\forall x,y\in V$, there holds:

$$\langle x - y, D(x) - D(y) \rangle \ge \gamma \|D(x) - D(y)\|^2. \tag{5}$$

Cocoercive operators are an important class of monotone operators. Many operators are cocoercive operators. Below are two typical cocoercive operators:

• D is firmly non-expansive: $(\forall x, y \in V)$

$$\langle x - y, D(x) - D(y) \rangle \ge \|D(x) - D(y)\|^2. \tag{6}$$

Such D is 1-cocoercive.

• D is residual non-expansive: $(\forall x, y \in V)$

$$\|(I - D) \circ (x) - (I - D) \circ (y)\| \le \|x - y\|.$$
 (7)

Such D is 0.5-cocoercive.

When $\gamma > 0$, cocoercive assumption make denoisers Lipschitz: by Cauchy-Schwarz inequality,

$$\langle x - y, D(x) - D(y) \rangle \le ||x - y|| ||D(x) - D(y)||.$$
 (8)

Therefore, by (5), $\|D(x) - D(y)\| \le \frac{1}{\gamma} \|x - y\|$, that is, D is $\frac{1}{\gamma}$ -Lipschitz. When $\gamma < 0.5$, both the operator and its residual part are expansive. In general, a smaller γ corresponds to less contraint, and therefore a more powerful denoiser.

Spectral analysis on D. Note that (5) can be equivalently transformed into the following inequality: $(\forall x, y \in V)$

$$\|(2\gamma D - I) \circ (x) - (2\gamma D - I) \circ (y)\| \le \|x - y\|. \tag{9}$$

Based on the mean value theorem [18], (9) is transformed into:

$$||2\gamma J(x) - I||_* \le 1, \forall x \in V, \tag{10}$$

where J(x) is the Fréchet differential, that is the Jacobian matrix when V is finite dimensional, of D at the point x, and $\|\cdot\|_*$ denotes the spectral norm. Since the spectral radius $\rho(\cdot)$ is always no larger than the spectral norm $\|\cdot\|_*$, we have that:

$$\rho(2\gamma J(x) - I) \le 1, \forall x \in V. \tag{11}$$

³Please note that, although we limit V to be finite dimensional for easy understanding, many theoretical analysis still hold in a general infinite dimensional real Hilbert space. To clarify, the spectrum set of an operator in a finite space is just the eigenvalue set. The transpose of a matrix in a finite dimensional space corresponds to the adjoint operator in an infinite space. $\|\cdot\|_*$ is the spectral norm in a finite space, and denotes the operator norm in an infinite space. The degradation operator K in an infinite space is assumed to be a bounded linear operator, that is $K \in \mathcal{B}[V]$.

⁴An operator in general may not be single-valued. However, since the operator D in this paper is a denoiser, its output is unique given fixed input. Thus, we only consider the single-valued operator here.

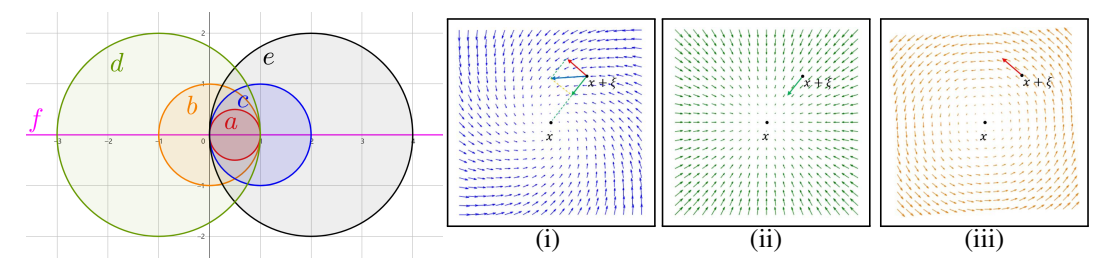


Figure 1: Left: Spectrum distributions of the Fréchet differential (Jacobian matrix) on the complex plane under different assumptions. (a) Firmly non-expansiveness, $\operatorname{Sp}(J) \subset \{z \in \mathbb{C} : |2z-1| \leq 1\}$; (b) Non-expansiveness, $\operatorname{Sp}(J) \subset \{z \in \mathbb{C} : |z| \leq 1\}$; (c) Residual non-expansiveness, $\operatorname{Sp}(J) \subset \{z \in \mathbb{C} : |z-1| \leq 1\}$; (d) $\frac{1}{2}$ -strictly pseudo-contractiveness, $\operatorname{Sp}(J) \subset \{z \in \mathbb{C} : |z+1| \leq 2\}$; (e) 0.25-cocoerciveness, $\operatorname{Sp}(J) \subset \{z \in \mathbb{C} : |0.5z-1| \leq 1\}$; (f) Conservativeness, $\operatorname{Sp}(J) \subset \mathbb{R}$. In general, a larger region means less restrictive assumption. The spectrum of γ -CoCo denoisers ($\gamma = 0.25$) lies inside the interval (f) \cap (e) = [0, 4]. Spectrum outside \mathbb{R} corresponds to the Hamiltonian part of the denoiser, and does not contribute to the denoising performance.

Right: A two-dimensional illustration of the Helmholtz decomposition of a denoiser D. x denotes the clean image point, ξ denotes the Gaussian noise, and $x+\xi$ denotes the noisy image. The arrow " \rightarrow " represents the denoising direction. (i) Denoising field D. (ii) Conservative field D_c . (iii) Hamiltonian field D_h .

Let $Sp(\cdot)$ denote the spectrum set, that is, the eigenvalue set when V is finte dimensional:

$$Sp(J) := \{ z \in \mathbb{C} : z I - J \text{ is not invertible} \}. \tag{12}$$

(11) implies $\operatorname{Sp}(J(x)) \subseteq \{z \in \mathbb{C} : |2\gamma z - 1| \le 1\}.$

Lemma 2.1 gives an *equivalent* condition of cocoerciveness in (5)-(9), and thereby enables the training through SR.

Lemma 2.1 (Proof in Appendix A.1). Let $D: V \to V$, and $J = \nabla D$ be its Fréchet differential. Then D is γ -cocoercive ($\gamma \in [0, \infty)$), if and only if $\|2\gamma J(x) - I\|_* \le 1$ for any $x \in V$.

Since the spectral radius is no larger than the spectral norm, we are able to plot the spectral distribution on the complex plane \mathbb{C} in Fig. 1. A larger region corresponds to a less restrictive constraint, and thus a better denoising performance. Figs. 1 (a), (c), (e) show that firm non-expansiveness, and residual non-expansiveness are special cases of cocoerciveness. Therefore, cocoeriveness is a weaker assumption for deep denoisers, and yields better denoising performance.

2.2 Conservative denoisers

We consider the conservative assumption intuitively. Let $D \in \mathcal{C}^1[V]$ be a denoiser. D is said to be conservative, if there is a potential function $\phi: V \to \overline{\mathbb{R}}$, such that $D = \nabla \phi$. Geometrically, D is mapping from V to V, thus can be viewed as a vector field.

By the generalized Helmholtz decomposition [8, 4], any vector field D can be decomposed into a conservative field D_c , and a Hamiltonian field D_h , such that D_c is curl-free and is the gradient of a potential function ϕ , and D_h is divergence-free:

$$D = D_c + D_h, D_c = \nabla \phi, \operatorname{div}(D_h) = 0.$$
(13)

However, the decomposition $D=D_c+D_h$ is implicit. In order to characterize this decomposition, we consider the Jacobian matrix J. The generalized Helmholtz decomposition can be rewritten as J=S+A, where $S=\frac{J+J^\top}{2}$ is symmetric, and $A=\frac{J-J^\top}{2}$ is anti-symmetric. S and A correspond to D_c and D_h respectively: $S=\nabla\,D_c$, $A=\nabla\,D_h$.

In Fig. 1, we consider a two-dimensional case. $x \in V$ is a clean image, ξ is the Gaussian noise with zero mean and standard derivation σ , $x + \xi$ is the noisy image. $\|x + \xi - x\| = \mathbb{E}[\|\xi\|] = 2\sigma$ is the distance between the clean image and the noisy image in V. A denoiser D is expected to reduce the distance as in Fig. 1 (i). That is $\|D(x + \xi) - x\| < \|x + \xi - x\|$. The arrow " \to " in Fig. 1 denotes the denoising direction vector η , $\eta = D(x + \xi) - (x + \xi)$. η can be decomposed into η_c and η_h , see

Figs. 1 (ii)-(iii). η_c points to the clean image, and thus represents the correct denoising direction. η_h circles around x, and D_h cannot remove noises.

In a general real Hilbert space, given a point $x, \forall y \in V$, define the Hamiltonian functional $\mathcal{H}(y) =$ $\frac{1}{2}\|D(y)-x\|^2$. When D is a Hamiltonian field, S=0. Then, the vector D(y)-x preserves the $\bar{\mathsf{le}}$ vel set of \mathcal{H} , because:

$$\langle \mathrm{D}(y) - x, \nabla_y \mathcal{H}(y) \rangle = \langle \mathrm{D}(y) - x, \mathrm{A}^\top (\mathrm{D}(y) - x) \rangle = 0.$$

Note that when x is a clean image, \mathcal{H} is a typical loss function for a denoiser. Therefore, a Hamiltonian field does not contribute to the denoising. Thus we penalize this useless part D_h by penalizing A. The following relations are useful: D is conservative \iff $D_h = 0 \iff A = 0 \iff \|J - J^{\top}\|_* = 0$.

In order to penalize D_h , we only need to minimize $\|J - J^\top\|_*$. Spectrally speaking, when $J = J^\top$ is self-adjoint, $Sp(J) \subset \mathbb{R}$, see Fig. 1 (f).

2.3 Characterization on CoCo denoisers

In the context of PnP, the denoiser D_{σ} is expected to be proximal. Building upon prior findings by [22] (see Appendix A.2), we present the following Theorem 2.2. A more general characterization on CoCo denoisers is given in Theorem A.5 in Appendix A.3.

Theorem 2.2 (Proof in Appendix A.4). Let $D_{\sigma} \in \mathcal{C}^1[V]$. $\beta = \frac{1}{\sigma^2}$. D_{σ} satisfies that:

- D_{σ} is conservative;
- D_{σ} is γ -cocoercive with $\gamma \in (0,1)$.

- Let $D_{\sigma}^t = t D_{\sigma} + (1-t) I$, $t \in [0,1)$. It holds that: there exists a r-weakly convex function $F: V \to \bar{\mathbb{R}}$, $r(t) = \beta \frac{t-\gamma t}{t+\gamma-\gamma t}$, such that $D_{\sigma}^t(x) \in$ $\operatorname{Prox}_{\frac{F}{2}}(x), \forall x \in V;$
- ∂F is L-Lipschitz, where

$$L(t) = \begin{cases} \beta \frac{t}{1-t} \ge r(t), & \text{if } t \ge \frac{1-2\gamma}{2-2\gamma} \text{ and } t \in [0,1) \text{ (Case 1)}; \\ r(t) = \beta \frac{t-\gamma t}{t+\gamma-\gamma t}, & \text{if } t \le \frac{1-2\gamma}{2-2\gamma} \text{ and } t \in [0,1) \text{ (Case 2)}. \end{cases}$$
(14)

Remark 2.3. D_{σ}^{t} is an averaged version of D_{σ} . As reported by [29], when D_{σ} is residual nonexpansive, PnP with D_{σ}^{t} out-performs PnP with D_{σ} in many inverse problems.

Remark 2.4. If $\gamma=0.5$, D_{σ} is residual non-expansive, D_{σ}^{t} is then residual t-Lipschitz, and $\beta^{-1}F$ is $\frac{t}{1+t}$ -weakly convex, with $\beta^{-1}\partial F$ being $\frac{t}{1-t}$ -Lipschitz. This special case recovers the result by [29].

Remark 2.5. By Theorem 2.2, we know that D_{σ}^{t} is a proximal operator of a weakly convex function $\frac{F}{3}$. We arrive at the following implicit non-convex restoration model:

$$\hat{u} \in \arg\min_{u \in V} F(u) + G(u; f), \ G(u; f) = \lambda \langle \mathbf{1}, Ku - f \log Ku \rangle. \tag{15}$$

Training strategy

Let θ be the parameter weights in D_{σ} to be optimized, π be the distribution of the training set of clean images, and $[\sigma_{\min}, \sigma_{\max}]$ be the interval of the noise level.

Based on Lemma 2.1 and the pioneer works by [66, 51], we encourage the cocoerciveness by the SR technique. The spectral regularization term L_s takes the form of:

$$L_s(\theta) = \mathbb{E}_{x,\sigma,\xi} \max\{\|2\gamma \mathbf{J} - \mathbf{I}\|_*, 1 - \epsilon\},\tag{16}$$

where θ is the network weights, $\epsilon \in (0,1)$ is a parameter that controls the constraint. $x \sim \pi, \sigma \sim$ $U[\sigma_{\min}, \sigma_{\max}], \xi \sim \mathcal{N}(0, \sigma^2 I). J = J(x + \xi) = \nabla D_{\sigma}(x + \xi; \theta).$

To encourage a conservative denoiser, we propose the Hamiltonian regularization term L_h :

$$L_h(\theta) = \mathbb{E}_{x,\sigma,\mathcal{E}} \| \mathbf{J} - \mathbf{J}^{\top} \|_*. \tag{17}$$

Combining (17) and (16), the overall loss function of D_{σ} is

$$Loss(\theta) = \mathbb{E} \| D_{\sigma}(x + \xi; \theta) - x \|_1 + \alpha_1 L_h + \alpha_2 L_s.$$
 (18)

 $\alpha_1, \alpha_2 > 0$ are balancing parameters. The first term in (97) ensures that D_σ is a Gaussian denoiser, the second term makes D_σ conservative, and the third term results in a γ -cocoercive denoiser. By minimizing $Loss(\theta)$, a properly regularized CoCo denoiser is obtained. Detailed calculation of $\|(2\gamma J - I)\|_*$ and $\|J - J^T\|_*$ is given in Appendix A.5.

4 PnP methods with CoCo denoisers

In order to solve the implicit nonconvex restoration model in (15), we first consider PnP-ADMM with CoCo denoisers, termed CoCo-ADMM. Then, we replace the fidelity term G in (15) by its Moreau envelope, and derive the proximal envelope gradient descent method (PEGD) with CoCo denoisers (CoCo-PEGD). The convergence are provided.

CoCo-ADMM. We first consider CoCo-ADMM iterations:

$$u^{k+1} = \operatorname{Prox}_{\frac{G}{\beta}}(v^k - b^k),$$

$$v^{k+1} = \operatorname{D}_{\sigma}^t(u^{k+1} + b^k),$$

$$b^{k+1} = b^k + u^{k+1} - v^{k+1},$$
(19)

where D^t_σ is defined in Theorem 2.2, and $\beta=\frac{1}{\sigma^2}$. The PnP-ADMM algorithm in (19) with a γ -CoCo denoiser is referred to as γ -CoCo-ADMM, or CoCo-ADMM for short.

When the denoiser $D_{\sigma} \in C^{1}[V]$ is a CoCo denoiser satisfying the conditions in Theorem 2.2, and F verifies the Kurdyka-Lojasiewicz (KL) property [1, 19], the global convergence of PnP-ADMM in (19) can be established as follows.

Theorem 4.1 (Proof in Appendix A.6). Let $F: V \to \overline{\mathbb{R}}$ be a coercive weakly convex KL function in Theorem 2.2 such that $D_{\sigma}^t \in \operatorname{Prox}_{\frac{F}{\beta}}$. $G: V \to \overline{\mathbb{R}}$ is lower semi-continuous and convex. $\gamma \in (0,1)$. $t \in [0,t_0)$, where $t_0 = t_0(\gamma)$ is the positive root of the equation

$$(2 - 2\gamma)t^3 + \gamma t^2 + 2\gamma t - \gamma = 0. (20)$$

Then, the sequence $\{(u^k, v^k, b^k)\}$ generated by (19) converges globally to a point (u^*, v^*, b^*) , and that $u^* = v^*$ is a stationary point of the model (15).

Remark 4.2. The KL property has been widely used to study the convergence of optimization algorithms in the nonconvex and nonsmooth setting [1]. Many functions, in particular all the real semi-algebraic functions, satisfy this property.

Remark 4.3. We consider several special cases of Theorem 4.1. Let D_{σ} be conservative. When $\gamma=0.5$, D_{σ} is residual non-expansive, and $t_0\approx 0.3761$. This recovers the case by [27]; when $\gamma=0.25$, both D_{σ} and its residual $I-D_{\sigma}$ can be expansive, but $0.5\,D_{\sigma}-I$ is non-expansive. In this case, $t_0\approx 0.3333$. When $\gamma=1$, D_{σ} is firmly non-expansive and is a proximal operator of some CCP function by Moreau's theorem. In this case, t_0 is no more needed to ensure the convergence, since this is the standard case of ADMM. In experiments, we use $D_{\sigma}(u^K+b^K)$ as the final output.

CoCo-PEGD. Now we consider the PGD algorithm with a CoCo denoiser. The standard PGD takes the form of:

$$u^{k+1} = \operatorname{Prox}_{\frac{F}{\beta}} \left(u^k - \beta^{-1} \nabla G(u^k) \right). \tag{21}$$

When F is r-weakly convex, ∇G is L_G -Lipschitz, and $\beta^{-1} < \max\{\frac{2}{L_G + r}, \frac{1}{L_G}\}$, the iteration (21) converges, see [2, 27].

However, in the Poisson inverse problems, G is not smooth, because ∇G is not Lipschitz. In order to apply the PGD algorithm, we smooth the fidelity G in (15) and (21) by replacing it with its Moreau envelope ${}^{\alpha}G$ ($\alpha \in (0,\infty)$): ${}^{\alpha}G(u) := \min_{v} G(v) + \frac{1}{2\alpha} \|v - u\|^2$.

Since G is CCP, ${}^{\alpha}G$ is differentiable [7]: $\nabla^{\alpha}G(u)=\frac{1}{\alpha}(\mathrm{I}-\mathrm{Prox}_{\alpha G})$, and that $\nabla^{\alpha}G$ is $\frac{1}{\alpha}$ -Lipschitz. Since there are already a step parameter β and a balancing parameter λ in G, throughout this paper, we set $\alpha=1$. Now the iteration becomes:

$$u^{k+1} = \text{Prox}_{\frac{F}{\beta}}(u^k - \beta^{-1}\nabla^1 G(u^k)).$$
 (22)

In (22), u alternates between a proximal operator $\operatorname{Prox}_{\frac{F}{\beta}}$, and a gradient descent step on the envelope of G. (22) is referred to as the proximal envelope gradient descent method (PEGD). Similar to

CoCo-ADMM (19), we replace $\operatorname{Prox}_{\frac{F}{\sigma}}$ with $\operatorname{D}_{\sigma}^{t}$, and arrive at CoCo-PEGD:

$$u^{k+1} = D_{\sigma}^{t}(u^{k} - \beta^{-1}\nabla^{1}G(u^{k})). \tag{23}$$

By Theorem 2.2, $D_{\sigma}^t = \operatorname{Prox}_{\frac{F}{\beta}}$, with F being r-weakly convex. Then by the Theorem 1 in [27], CoCo-PEGD converges when $\beta^{-1} < \max\{\frac{2}{1+r}, 1\}$. This convergence result is summarized in Theorem 4.4. By Theorem 4.4, when $\beta > 1$, CoCo-PEGD converges.

Theorem 4.4 (Proof in Appendix A.7). Let $F: V \to \overline{\mathbb{R}}$ be a coercive r-weakly convex KL function in Theorem 2.2 such that $D_{\sigma}^t = \operatorname{Prox}_{\frac{F}{\beta}}$. $G: V \to \overline{\mathbb{R}}$ is CCP. $\gamma \in [0.25, 1]$. $t \in (0, 1]$. $0 < \beta^{-1} < \max\{\frac{2}{1+r}, 1\}$. Then the sequence $\{u^k\}$ generated in (23) converges to a stationary point of:

$$\hat{u} \in \arg\min_{u \in V} F(u) + {}^{1}G(u; f). \tag{24}$$

5 Experiments

All the experiments are conducted under Linux system, Python 3.8.12 and Pytorch 1.10.2 with a RTX 3090 GPU.

Training details. For D_{σ} , we select DRUNet [73], which combines a residual learning [24] and UNet architecture [58]. DRUNet takes both the noisy image and the noise level σ as input, making it convenient for PnP image restoration.

To train a CoCo denoiser, we collect 800 images from the DIV2K dataset [30] as the training set and used a batch size of 32 and patch size 128. We add Gaussian noise with randomly generated standard deviation values in the range of $[\sigma_{\min}, \sigma_{\max}] = [0, 50]$ to the clean image. Adam optimizer is applied to train the model with learning rate $lr = 10^{-4}$. We set $\alpha_1 = 1, \alpha_2 = 0.01$, and $\epsilon = 0.1$ to ensure the regularity conditions. To accurately evaluate the spectral norms $\|J(x) - J^{T}(x)\|_{*}$ and $\|(2\gamma J - I)(x)\|_{*}$, we use the power iterative method [21] with 30 iterations to ensure the convergence.

Denoising performance. We evaluate the Gaussian denoising performances of the proposed denoiser CoCo-DRUNet, strictly pseudo-contractive DRUNet (SPC-DRUNet) [71], resolvent of a maximally monotone operator (RMMO) [51] which is firmly non-expansive, GS-DRUNet [28], Prox-DRUNet [29], the standard DRUNet, FFDNet [75], and DnCNN [74].

The PSNR values are given in Table 1. A γ -cocoercive conservative denoiser is referred to as γ -CoCo-DRUNet. We see in Table 1 that compared with DnCNN, FFDNet, and the regularized denoisers, 0.25-CoCo-DRUNet has competitive denoising performance. This is because that: cocoercive and conservative properties are less restrictive for deep denoisers; denoiser is trained with a different loss function. Both 0.50-CoCo-DRUNet and Prox-DRUNet are conservative with non-expansive residual, and therefore share a similar denoising performance.

Table 1: Left: Average denoising PSNR performance of different denoisers on CBSD68, for various noise levels σ ; Right: Mean symmetry error $\parallel J - J^{\top} \parallel_* (N=1)$ and maximal values of the norm $\parallel 2\gamma J - I \parallel_* (N=30)$ for various noise levels σ and $\gamma = 0.50, 0.25$.

	$\sigma = 15$	$\sigma = 25$	$\sigma = 40$
FFDNet	33.86	31.18	28.81
DnCNN	33.88	31.20	28.89
DRUNet	34.14	31.54	29.33
RMMO	32.21	29.99	27.87
GS-DRUNet	33.56	31.01	28.81
Prox-DRUNet	33.18	30.60	28.38
SPC-DRUNet	33.90	31.29	29.10
0.50-CoCo-DRUNet	33.38	30.65	28.25
0.25-CoCo-DRUNet	34.00	31.38	29.16

	15	25	40	Norms
DRUNet	4.1e+0	4.2e+1	1.8e+1	$\parallel \mathbf{J} - \mathbf{J}^{\top} \parallel_{*}$
0.50-CoCo-DRUNet	8.6e-3	2.5e-4	7.1e-4	$\ \mathbf{J} - \mathbf{J}^{\top}\ _{*}$
$0.25 ext{-CoCo-DRUNet}$	3.1e-4	1.8e-4	3.9e-4	$\ \operatorname{J}-\operatorname{J}^{\top}\ _*$
DRUNet	3.285	4.343	6.283	$\ { m J} - { m I} \ _*$
0.50-CoCo-DRUNet	0.994	0.992	0.972	$ J - I _*$
0.25-CoCo-DRUNet	0.986	0.969	0.982	$\ 0.5 \mathrm{J} - 1\ _*$

Assumption validations. In the experiments, the symmetric Jacobian and non-expansive residual are softly constrained by the loss function (97) with trade-off parameters α_1,α_2 . We validate the conditions in Table 1. We use the symmetry error $\|\operatorname{J}(x)-\operatorname{J}^\top(x)\|_*$ over 100 different patches with N=1 as in Algorithm 1 for better demonstration. A smaller error denotes a higher Jacobian symmetry. The cocoerciveness is validated by calculating $\|2\gamma\operatorname{J}(x)-x\|_*$. If $\|2\gamma\operatorname{J}(x)-x\|_* \leq 1$, the denoiser is γ -cocoercive.

As shown in Table 1, DRUNet without regularization terms has an expansive residual part. The regularized CoCo-DRUNet is cocoercive. Besides, the proposed Hamiltonian regularization term indeed encourages a symmetric Jacobian: in Table 1, we see that Hamiltonian regularization reduces the symmetry error. It validates the effectiveness of the proposed training strategy. Ablation study on the parameters α_1 and α_2 in (97) are provided on Appendix A.16.

PnP restoration. We apply CoCo-ADMM and CoCo-PEGD to multiple Poisson inverse problems including: **photon limited deconvolution**, **single photon imaging** in a real-world low-light setting in Appendix A.10, **low-dose CT reconstruction** tasks in Appendix A.12, **Poisson denoising** in Appendix A.13. **Computational time**, **performances under extreme conditions**, and **blind deblur and denoise results**, are reported in Appendices A.14, A.15, A.17, and A.18 respectively.

When K in (2) is not the identity matrix, in general, $Prox_G$ has no closed-form solution. Since G is convex, we use ADMM to solve $Prox_G$ efficiently. For details, please refer to Appendix A.8.

We choose $\gamma=0.25$ since 0.25-CoCo-DRUNet has a satisfactory performance. According to Theorems 4.1-4.4, CoCo-ADMM and CoCo-PEGD are guaranteed to converge with t<0.3333. For both CoCo-ADMM and PEGD, we need to calculate the proximal operator $\operatorname{Prox}_{\frac{G}{\beta}}$. We detail the calculations for each task in Appendix A.8. For each method, we fine tune the parameters to achieve the best quantitive PSNR values. The proposed methods are initialized with the observed image, that is $u^0=v^0=f, b^0=0$.

Table 2: Left: Average deconvolution PSNR and SSIM performance by different methods on CBSD68 with Levin's 8 kernels and Poisson noises with peak value p=50 and p=100. Right: Average low-dose CT reconstruction PSNR and SSIM performance by different methods on Mayo's dataset with Poisson noises with peak value p=500, and p=100.

	p =	100	p = 50		
	PSNR	SSIM	PSNR	SSIM	
DPIR	26.51	0.7419	25.38	0.6910	
RMMO-DRS	25.94	0.7019	25.10	0.6546	
Prox-DRS	25.68	0.6764	25.21	0.6572	
DPS	23.65	0.6062	23.10	0.5816	
DiffPIR	24.82	0.6429	24.08	0.6074	
SNORE	26.33	0.7158	25.21	0.6719	
PnPI-HQS	26.42	0.7158	25.61	0.6956	
B-RED	24.09	0.6794	23.78	0.6603	
CoCo-ADMM	26.89	0.7358	26.00	0.7026	
CoCo-PEGD	26.79	0.7323	25.90	0.6958	

	p =	500	p = 100		
	PSNR	SSIM	PSNR	SSIM	
FBP	28.76	0.5212	24.10	0.2974	
PWLS-TGV	33.16	0.8461	30.43	0.7750	
PWLS-CSCGR	35.45	0.8909	33.78	0.8534	
UNet	36.93	0.9139	35.19	0.8875	
WNet	37.12	0.9266	35.98	0.9130	
CoCo-ADMM	37.63	0.9403	36.68	0.9194	
CoCo-PEGD	37.72	0.9391	<u>36.43</u>	<u>0.9159</u>	

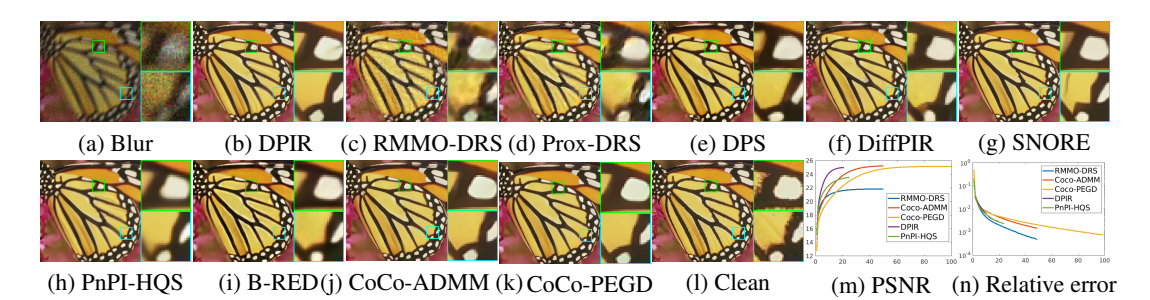


Figure 2: Deconvolution results by different methods on the image 'Butterfly' from Set3c with kernel 2 and p=50 Poisson noises. (a) Blur image. (b) DPIR, PSNR=25.00dB. (c) RMMO-DRS, PSNR=21.86dB. (d) Prox-DRS, PSNR=22.57dB. (e) DPS, PSNR=21.47dB. (f) Diff-PIR, PSNR=22.66dB. (g) SNORE, PSNR=25.14dB. (h) PnPI-HQS, PSNR=23.56dB. (i) B-RED, PSNR=23.34dB. (j) CoCo-ADMM, PSNR=25.25dB. (k) CoCo-PEGD, PSNR=25.17dB. (l) Clean image. (m) PSNR curves. (n) Relative error curves. x-axis denotes the iteration number.

Photon limited deconvolution. In this task, K in (15) is the blur kernel. We use 8 real-world camera shake kernels by [39], see Fig. 4 in Appendix A.9.

We compare our methods with some close related PnP methods, including DPIR [73], which applies PnP-HQS method with decreasing step size. Please note that DPIR is not guaranteed to converge;

RMMO-DRS [66], which uses the DRS method with a firmly non-expansive denoiser RMMO; B-RED [27], which uses the gradient descent method with a Bregman denoiser; PnPI-HQS [71], which uses the Ishikawa HQS method with a strictly pseudo-contractive denoiser; SNORE [55], which proposes the novel stochastic denoising regularization by iteratively adding Gaussian noises. We also compare two state-of-the-art diffusion-based methods: DPS [15] and DiffPIR [77]. The average PSNR and SSIM values on CBSD68 are summarized in Table 2.

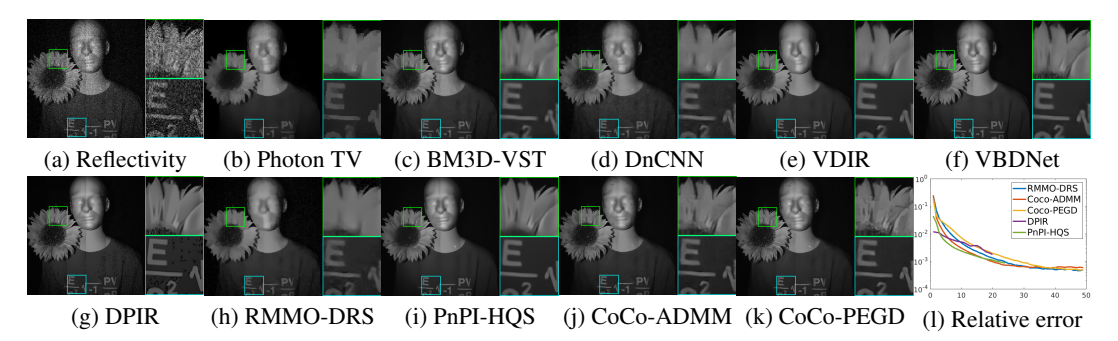


Figure 3: Single photon imaging results in a real-world low light setting by different methods.

We show the visual results in Fig. 2. In Fig. 2 (a), the image 'Butterfly' is severely degraded. In this setting, many methods fail to recover the clear edges, see Figs. 2 (c)-(i). Compared with DPIR and SNORE, the enlarged parts by CoCo-ADMM and CoCo-PEGD are closer to the potential clean image, see Figs. 2 (b), (e), (h), (i).

6 Conclusion and Limitation

This paper introduces a novel cocoercive conservative assumption on the denoiser. Cocoerciveness is weaker than the existing assumptions, and is less restrictive for a deep denoiser. Conservativeness is analyzed geometrically by the generalized Helmholtz decomposition on the Fréchet differential. We propose a novel training strategy that incorporates a Hamiltonian regularization term and a spectral regularization term, which encourages a cocoercive conservative (CoCo) Gaussian denoiser. Theoretically, CoCo denoiser is proved to be a proximal operator of an implicit weakly convex prior function. The global convergence results of PnP methods to a stationary point are given. The results can be naturally generalized to other inverse problems with a convex fidelity term and an implicit weakly convex prior term. Extensive experimental results demonstrate that the proposed CoCo-PnP methods achieve competitive performance in terms of both visual quality and quantitative measures.

The main limitation of this paper is that the proposed CoCo denoiser exhibits a slightly worse Gaussian denoising performance compared to the non-regularized denoiser, see Table 6. This is because the proposed regularized denoiser sacrifices a little denoising performance in order to achieve guaranteed theoretical results as stated in Theorems 2.2-4.4. Another limitation is that the proposed learning strategy can only encourage the desired mathematical properties, not enforce them. In experiments, we do observe that sometimes, even after a long time spectral regularization training, the trained denoiser still violates the cocoercive property on some particular images. For conservativity, we find that when N=30, the symmetry error compared with standard DRUNet is smaller, but not significantly smaller. How to enforce such properties without greatly compromising the denoising performance is still an open problem. Since the paper mainly focuses on the theoretical analysis of PnP methods, we will address these limitations in future works.

Acknowledgments

Fang Li is supported by National Key R&D Program of China (Nos. 2021YFA1000302), Fundamental Research Funds for the Central Universities, Natural Science Foundation of Shanghai (No. 22ZR1419500), Science and Technology Commission of Shanghai Municipality (No. 22DZ2229014), and Natural Science Foundation of Chongqing, China (No. CSTB2023NSCQ-MSX0276). Tieyong Zeng is supported in part by BNBU Research Grant (No. UICR0100031, UICR0700108-25 and UICR0900003) at Beijing Normal-Hong Kong Baptist University, Zhuhai, PR China.

References

- [1] Hédy Attouch, Jérôme Bolte, Patrick Redont, and Antoine Soubeyran. Proximal alternating minimization and projection methods for nonconvex problems: An approach based on the kurdyka-łojasiewicz inequality. *Mathematics of operations research*, 35(2):438–457, 2010.
- [2] Hedy Attouch, Jérôme Bolte, and Benar Fux Svaiter. Convergence of descent methods for semi-algebraic and tame problems: proximal algorithms, forward–backward splitting, and regularized gauss–seidel methods. *Mathematical Programming*, 137(1):91–129, 2013.
- [3] Lucio Azzari and Alessandro Foi. Variance stabilization for noisy+ estimate combination in iterative poisson denoising. *IEEE signal processing letters*, 23(8):1086–1090, 2016.
- [4] David Balduzzi, Sebastien Racaniere, James Martens, Jakob Foerster, Karl Tuyls, and Thore Graepel. The mechanics of n-player differentiable games. In *International Conference on Machine Learning*, pages 354–363. PMLR, 2018.
- [5] Peng Bao, Wenjun Xia, Kang Yang, Weiyan Chen, Mianyi Chen, Yan Xi, Shanzhou Niu, Jiliu Zhou, He Zhang, Huaiqiang Sun, et al. Convolutional sparse coding for compressed sensing ct reconstruction. *IEEE transactions on medical imaging*, 38(11):2607–2619, 2019.
- [6] Heinz H Bauschke and Patrick L Combettes. The baillon-haddad theorem revisited. *Journal of Convex Analysis*, 17(3&4):781–787, 2010.
- [7] Heinz H Bauschke, Patrick L Combettes, Heinz H Bauschke, and Patrick L Combettes. *Correction to: convex analysis and monotone operator theory in Hilbert spaces*. Springer, 2017.
- [8] Harsh Bhatia, Gregory Norgard, Valerio Pascucci, and Peer-Timo Bremer. The helmholtz-hodge decomposition—a survey. *IEEE Transactions on visualization and computer graphics*, 19(8):1386–1404, 2012.
- [9] Charles A Bouman and Gregery T Buzzard. Generative plug and play: Posterior sampling for inverse problems. In 2023 59th Annual Allerton Conference on Communication, Control, and Computing (Allerton), pages 1–7. IEEE, 2023.
- [10] Stephen Boyd, Neal Parikh, Eric Chu, Borja Peleato, Jonathan Eckstein, et al. Distributed optimization and statistical learning via the alternating direction method of multipliers. *Foundations and Trends® in Machine learning*, 3(1):1–122, 2011.
- [11] Kristian Bredies, Karl Kunisch, and Thomas Pock. Total generalized variation. *SIAM Journal on Imaging Sciences*, 3(3):492–526, 2010.
- [12] Gregery T Buzzard, Stanley H Chan, Suhas Sreehari, and Charles A Bouman. Plug-and-play unplugged: Optimization-free reconstruction using consensus equilibrium. SIAM Journal on Imaging Sciences, 11(3), 2018.
- [13] Stanley H Chan, Xiran Wang, and Omar A Elgendy. Plug-and-play admm for image restoration: Fixed-point convergence and applications. *IEEE Transactions on Computational Imaging*, 3(1):84–98, 2016.
- [14] Theodor Cheslerean-Boghiu, Felix C Hofmann, Manuel Schultheiß, Franz Pfeiffer, Daniela Pfeiffer, and Tobias Lasser. Wnet: A data-driven dual-domain denoising model for sparse-view computed tomography with a trainable reconstruction layer. *IEEE Transactions on Computational Imaging*, 9:120–132, 2023.
- [15] Hyungjin Chung, Jeongsol Kim, Michael T Mccann, Marc L Klasky, and Jong Chul Ye. Diffusion posterior sampling for general noisy inverse problems. *The Eleventh International Conference on Learning Representations*, 2023.
- [16] Regev Cohen, Yochai Blau, Daniel Freedman, and Ehud Rivlin. It has potential: Gradient-driven denoisers for convergent solutions to inverse problems. *Advances in Neural Information Processing Systems*, 34:18152–18164, 2021.

- [17] Weisheng Dong, Tao Huang, Guangming Shi, Yi Ma, and Xin Li. Robust tensor approximation with laplacian scale mixture modeling for multiframe image and video denoising. *IEEE Journal of Selected Topics in Signal Processing*, 12(6):1435–1448, 2018.
- [18] Johannes Jisse Duistermaat and Johan AC Kolk. *Multidimensional real analysis I: differentiation*, volume 86. Cambridge University Press, 2004.
- [19] Pierre Frankel, Guillaume Garrigos, and Juan Peypouquet. Splitting methods with variable metric for kurdyka–łojasiewicz functions and general convergence rates. *Journal of Optimization Theory and Applications*, 165:874–900, 2015.
- [20] Antonio Galbis and Manuel Maestre. Vector analysis versus vector calculus. Springer Science & Business Media, 2012.
- [21] Gene H Golub and Charles F Van Loan. Matrix computations. JHU press, 2013.
- [22] Rémi Gribonval and Mila Nikolova. A characterization of proximity operators. *Journal of Mathematical Imaging and Vision*, 62(6):773–789, 2020.
- [23] Shuhang Gu, Lei Zhang, Wangmeng Zuo, and Xiangchu Feng. Weighted nuclear norm minimization with application to image denoising. In *Proceedings of the IEEE conference on computer vision and pattern recognition*, pages 2862–2869, 2014.
- [24] Kaiming He, Xiangyu Zhang, Shaoqing Ren, and Jian Sun. Deep residual learning for image recognition. In *Proceedings of the IEEE conference on computer vision and pattern recognition*, pages 770–778, 2016.
- [25] Felix Heide, Markus Steinberger, Yun-Ta Tsai, Mushfiqur Rouf, Dawid Pająk, Dikpal Reddy, Orazio Gallo, Jing Liu, Wolfgang Heidrich, Karen Egiazarian, et al. Flexisp: A flexible camera image processing framework. *ACM Transactions on Graphics (ToG)*, 33(6):1–13, 2014.
- [26] Werner Heisenberg. Über den anschaulichen inhalt der quantentheoretischen kinematik und mechanik. *Zeitschrift für Physik*, 43(3):172–198, 1927.
- [27] Samuel Hurault, Antonin Chambolle, Arthur Leclaire, and Nicolas Papadakis. Convergent plug-and-play with proximal denoiser and unconstrained regularization parameter. *Journal of Mathematical Imaging and Vision*, pages 1–23, 2024.
- [28] Samuel Hurault, Arthur Leclaire, and Nicolas Papadakis. Gradient step denoiser for convergent plug-and-play. In *International Conference on Learning Representations (ICLR*'22), 2022.
- [29] Samuel Hurault, Arthur Leclaire, and Nicolas Papadakis. Proximal denoiser for convergent plug-and-play optimization with nonconvex regularization. In *International Conference on Machine Learning*, pages 9483–9505. PMLR, 2022.
- [30] Andrey Ignatov, Radu Timofte, et al. Pirm challenge on perceptual image enhancement on smartphones: report. In European Conference on Computer Vision (ECCV) Workshops, January 2019.
- [31] Kyong Hwan Jin, Michael T McCann, Emmanuel Froustey, and Michael Unser. Deep convolutional neural network for inverse problems in imaging. *IEEE transactions on image processing*, 26(9):4509–4522, 2017.
- [32] Ulugbek S Kamilov, Charles A Bouman, Gregery T Buzzard, and Brendt Wohlberg. Plug-and-play methods for integrating physical and learned models in computational imaging: Theory, algorithms, and applications. *IEEE Signal Processing Magazine*, 40(1):85–97, 2023.
- [33] Stefan Kindermann, Stanley Osher, and Peter W Jones. Deblurring and denoising of images by nonlocal functionals. *Multiscale Modeling & Simulation*, 4(4):1091–1115, 2005.
- [34] Prashanth G Kumar and Rajiv Ranjan Sahay. Low rank poisson denoising (lrpd): A low rank approach using split bregman algorithm for poisson noise removal from images. In *Proceedings of the IEEE/CVF Conference on Computer Vision and Pattern Recognition Workshops*, 2019.

- [35] Wei-Sheng Lai, Jia-Bin Huang, Zhe Hu, Narendra Ahuja, and Ming-Hsuan Yang. A comparative study for single image blind deblurring. In *Proceedings of the IEEE Conference on Computer Vision and Pattern Recognition*, pages 1701–1709, 2016.
- [36] Charles Laroche, Andrés Almansa, Eva Coupeté, and Matias Tassano. Provably convergent plug & play linearized admm, applied to deblurring spatially varying kernels. In *ICASSP 2023-2023 IEEE International Conference on Acoustics, Speech and Signal Processing (ICASSP)*, pages 1–5. IEEE, 2023.
- [37] Charles Laroche, Andrés Almansa, and Matias Tassano. Deep model-based super-resolution with non-uniform blur. In *Proceedings of the IEEE/CVF Winter Conference on Applications of Computer Vision*, pages 1797–1808, 2023.
- [38] Mikael Le Pendu and Christine Guillemot. Preconditioned plug-and-play admm with locally adjustable denoiser for image restoration. *SIAM Journal on Imaging Sciences*, 16(1):393–422, 2023.
- [39] Anat Levin, Yair Weiss, Fredo Durand, and William T Freeman. Understanding and evaluating blind deconvolution algorithms. In 2009 IEEE conference on computer vision and pattern recognition, pages 1964–1971. IEEE, 2009.
- [40] Guoyin Li and Ting Kei Pong. Douglas—rachford splitting for nonconvex optimization with application to nonconvex feasibility problems. *Mathematical programming*, 159:371–401, 2016.
- [41] Hao Liang, Rui Liu, Zhongyuan Wang, Jiayi Ma, and Xin Tian. Variational bayesian deep network for blind poisson denoising. *Pattern Recognition*, 143:109810, 2023.
- [42] Jun Liu, Ming Yan, and Tieyong Zeng. Surface-aware blind image deblurring. *IEEE Transactions on Pattern Analysis and Machine Intelligence*, 43(3):1041–1055, 2019.
- [43] Wei Liu and Weisi Lin. Additive white gaussian noise level estimation in svd domain for images. *IEEE Transactions on Image processing*, 22(3):872–883, 2012.
- [44] Ponce J et al. Mairal J, Bach F. Non-local sparse models for image restoration. *IEEE 12th International Conference on Computer Vision*, pages 2272–2279, 2009.
- [45] MayoClinic. The 2016 nih-aapm-mayo clinic low dose ct grand challenge, http://www.aapm.org/grandchallenge/lowdosect/. 2016.
- [46] Taylor R et al. Moen. Low-dose ct image and projection dataset. *Medical Physics*, 48(2):902–911, 2021.
- [47] Jean-Jacques Moreau. Proximité et dualité dans un espace hilbertien. *Bulletin de la Société mathématique de France*, 93:273–299, 1965.
- [48] Shanzhou Niu, Yang Gao, Zhaoying Bian, Jing Huang, Wufan Chen, Gaohang Yu, Zhengrong Liang, and Jianhua Ma. Sparse-view x-ray ct reconstruction via total generalized variation regularization. *Physics in Medicine & Biology*, 59(12):2997, 2014.
- [49] Jinshan Pan, Zhe Hu, Zhixun Su, and Ming-Hsuan Yang. *l*_0-regularized intensity and gradient prior for deblurring text images and beyond. *IEEE transactions on pattern analysis and machine intelligence*, 39(2):342–355, 2016.
- [50] Adam Paszke, Sam Gross, Soumith Chintala, Gregory Chanan, Edward Yang, Zachary DeVito, Zeming Lin, Alban Desmaison, Luca Antiga, and Adam Lerer. Automatic differentiation in pytorch. 2017.
- [51] Jean-Christophe Pesquet, Audrey Repetti, Matthieu Terris, and Yves Wiaux. Learning maximally monotone operators for image recovery. SIAM Journal on Imaging Sciences, 14(3):1206–1237, 2021.
- [52] Tobias Plötz and Stefan Roth. Benchmarking denoising algorithms with real photographs. *CVPR*, 2017.

- [53] Blanca Priego, Richard J Duro, and Jocelyn Chanussot. 4dcaf: A temporal approach for denoising hyperspectral image sequences. *Pattern Recognition*, 72:433–445, 2017.
- [54] Edward T Reehorst and Philip Schniter. Regularization by denoising: Clarifications and new interpretations. *IEEE transactions on computational imaging*, 5(1):52–67, 2018.
- [55] Marien Renaud, Jean Prost, Arthur Leclaire, and Nicolas Papadakis. Plug-and-play image restoration with stochastic denoising regularization. In Forty-first International Conference on Machine Learning, 2024.
- [56] Howard Percy Robertson. The uncertainty principle. *Physical Review*, 34(1):163, 1929.
- [57] Yaniv Romano, Michael Elad, and Peyman Milanfar. The little engine that could: Regularization by denoising (red). *SIAM Journal on Imaging Sciences*, 10(4):1804–1844, 2017.
- [58] Olaf Ronneberger, Philipp Fischer, and Thomas Brox. U-net: Convolutional networks for biomedical image segmentation. In *Medical Image Computing and Computer-Assisted Intervention–MICCAI 2015: 18th International Conference, Munich, Germany, October 5-9, 2015, Proceedings, Part III 18*, pages 234–241. Springer, 2015.
- [59] Leonid I Rudin, Stanley Osher, and Emad Fatemi. Nonlinear total variation based noise removal algorithms. *Physica D: nonlinear phenomena*, 60(1-4):259–268, 1992.
- [60] Ernest Ryu, Jialin Liu, Sicheng Wang, Xiaohan Chen, Zhangyang Wang, and Wotao Yin. Plug-and-play methods provably converge with properly trained denoisers. In *International Conference on Machine Learning*, pages 5546–5557. PMLR, 2019.
- [61] Tim Salimans and Jonathan Ho. Should ebms model the energy or the score? In Energy Based Models Workshop-ICLR 2021, 2021.
- [62] Dongeek Shin, Feihu Xu, Dheera Venkatraman, Rudi Lussana, Federica Villa, Franco Zappa, Vivek K Goyal, Franco NC Wong, and Jeffrey H Shapiro. Photon-efficient imaging with a single-photon camera. *Nature communications*, 7(1):12046, 2016.
- [63] Jae Woong Soh and Nam Ik Cho. Variational deep image restoration. *IEEE Transactions on Image Processing*, 31:4363–4376, 2022.
- [64] Suhas Sreehari, S Venkat Venkatakrishnan, Brendt Wohlberg, Gregery T Buzzard, Lawrence F Drummy, Jeffrey P Simmons, and Charles A Bouman. Plug-and-play priors for bright field electron tomography and sparse interpolation. *IEEE Transactions on Computational Imaging*, 2(4):408–423, 2016.
- [65] Yu Sun, Brendt Wohlberg, and Ulugbek S Kamilov. An online plug-and-play algorithm for regularized image reconstruction. *IEEE Transactions on Computational Imaging*, 5(3):395–408, 2019.
- [66] Matthieu Terris, Audrey Repetti, Jean-Christophe Pesquet, and Yves Wiaux. Building firmly nonexpansive convolutional neural networks. In ICASSP 2020-2020 IEEE International Conference on Acoustics, Speech and Signal Processing (ICASSP), pages 8658–8662. IEEE, 2020.
- [67] DNH Thanh and SD Dvoenko. A denoising of biomedical images. *The International Archives of the Photogrammetry, Remote Sensing and Spatial Information Sciences*, 40:73–78, 2015.
- [68] Andreas Themelis and Panagiotis Patrinos. Douglas—rachford splitting and admm for nonconvex optimization: Tight convergence results. SIAM Journal on Optimization, 30(1):149–181, 2020.
- [69] Singanallur V Venkatakrishnan, Charles A Bouman, and Brendt Wohlberg. Plug-and-play priors for model based reconstruction. In 2013 IEEE global conference on signal and information processing, pages 945–948. IEEE, 2013.
- [70] Jianyi Wang, Kelvin CK Chan, and Chen Change Loy. Exploring clip for assessing the look and feel of images. In *Proceedings of the AAAI conference on artificial intelligence*, volume 37, pages 2555–2563, 2023.

- [71] Deliang Wei, Peng Chen, and Fang Li. Learning pseudo-contractive denoisers for inverse problems. In *Proceedings of the 41st International Conference on Machine Learning*, volume 235 of *Proceedings of Machine Learning Research*, pages 52500–52524. PMLR, 21–27 Jul 2024.
- [72] Deliang Wei, Fang Li, Shen Xiao, and Tieyong Zeng. Deepspim: Deep semi-proximal iterative method for sparse-view ct reconstruction with convergence guarantee. *CSIAM Transactions on Applied Mathematics*, 5(3):421–447, 2024.
- [73] Kai Zhang, Yawei Li, Wangmeng Zuo, Lei Zhang, Luc Van Gool, and Radu Timofte. Plug-and-play image restoration with deep denoiser prior. *IEEE Transactions on Pattern Analysis and Machine Intelligence*, 44(10):6360–6376, 2021.
- [74] Kai Zhang, Wangmeng Zuo, Yunjin Chen, Deyu Meng, and Lei Zhang. Beyond a gaussian denoiser: Residual learning of deep cnn for image denoising. *IEEE transactions on image processing*, 26(7):3142–3155, 2017.
- [75] Kai Zhang, Wangmeng Zuo, and Lei Zhang. Ffdnet: Toward a fast and flexible solution for cnn-based image denoising. *IEEE Transactions on Image Processing*, 27(9):4608–4622, 2018.
- [76] Tianjing Zhang, Yuhui Quan, and Hui Ji. Cross-scale self-supervised blind image deblurring via implicit neural representation. In *The Thirty-eighth Annual Conference on Neural Information Processing Systems*, 2024.
- [77] Yuanzhi Zhu, Kai Zhang, Jingyun Liang, Jiezhang Cao, Bihan Wen, Radu Timofte, and Luc Van Gool. Denoising diffusion models for plug-and-play image restoration. In *Proceedings of the IEEE/CVF Conference on Computer Vision and Pattern Recognition*, pages 1219–1229, 2023.

NeurIPS Paper Checklist

1. Claims

Question: Do the main claims made in the abstract and introduction accurately reflect the paper's contributions and scope?

Answer: [Yes]

Justification: In the abstract and the introduction part, we have claimed the contributions clearly.

Guidelines:

- The answer NA means that the abstract and introduction do not include the claims made in the paper.
- The abstract and/or introduction should clearly state the claims made, including the contributions made in the paper and important assumptions and limitations. A No or NA answer to this question will not be perceived well by the reviewers.
- The claims made should match theoretical and experimental results, and reflect how much the results can be expected to generalize to other settings.
- It is fine to include aspirational goals as motivation as long as it is clear that these goals are not attained by the paper.

2. Limitations

Question: Does the paper discuss the limitations of the work performed by the authors?

Answer: [Yes]

Justification: We have included a limitation section.

Guidelines:

- The answer NA means that the paper has no limitation while the answer No means that the paper has limitations, but those are not discussed in the paper.
- The authors are encouraged to create a separate "Limitations" section in their paper.
- The paper should point out any strong assumptions and how robust the results are to violations of these assumptions (e.g., independence assumptions, noiseless settings, model well-specification, asymptotic approximations only holding locally). The authors should reflect on how these assumptions might be violated in practice and what the implications would be.
- The authors should reflect on the scope of the claims made, e.g., if the approach was only tested on a few datasets or with a few runs. In general, empirical results often depend on implicit assumptions, which should be articulated.
- The authors should reflect on the factors that influence the performance of the approach.
 For example, a facial recognition algorithm may perform poorly when image resolution
 is low or images are taken in low lighting. Or a speech-to-text system might not be
 used reliably to provide closed captions for online lectures because it fails to handle
 technical jargon.
- The authors should discuss the computational efficiency of the proposed algorithms and how they scale with dataset size.
- If applicable, the authors should discuss possible limitations of their approach to address problems of privacy and fairness.
- While the authors might fear that complete honesty about limitations might be used by reviewers as grounds for rejection, a worse outcome might be that reviewers discover limitations that aren't acknowledged in the paper. The authors should use their best judgment and recognize that individual actions in favor of transparency play an important role in developing norms that preserve the integrity of the community. Reviewers will be specifically instructed to not penalize honesty concerning limitations.

3. Theory assumptions and proofs

Question: For each theoretical result, does the paper provide the full set of assumptions and a complete (and correct) proof?

Answer: [Yes]

Justification: We have provided detailed and correct proofs for each theoretical results. Guidelines:

- The answer NA means that the paper does not include theoretical results.
- All the theorems, formulas, and proofs in the paper should be numbered and cross-referenced.
- All assumptions should be clearly stated or referenced in the statement of any theorems.
- The proofs can either appear in the main paper or the supplemental material, but if they appear in the supplemental material, the authors are encouraged to provide a short proof sketch to provide intuition.
- Inversely, any informal proof provided in the core of the paper should be complemented by formal proofs provided in appendix or supplemental material.
- Theorems and Lemmas that the proof relies upon should be properly referenced.

4. Experimental result reproducibility

Question: Does the paper fully disclose all the information needed to reproduce the main experimental results of the paper to the extent that it affects the main claims and/or conclusions of the paper (regardless of whether the code and data are provided or not)?

Answer: [Yes]

Justification: We have clearly stated the experimental settings.

Guidelines:

- The answer NA means that the paper does not include experiments.
- If the paper includes experiments, a No answer to this question will not be perceived well by the reviewers: Making the paper reproducible is important, regardless of whether the code and data are provided or not.
- If the contribution is a dataset and/or model, the authors should describe the steps taken to make their results reproducible or verifiable.
- Depending on the contribution, reproducibility can be accomplished in various ways. For example, if the contribution is a novel architecture, describing the architecture fully might suffice, or if the contribution is a specific model and empirical evaluation, it may be necessary to either make it possible for others to replicate the model with the same dataset, or provide access to the model. In general, releasing code and data is often one good way to accomplish this, but reproducibility can also be provided via detailed instructions for how to replicate the results, access to a hosted model (e.g., in the case of a large language model), releasing of a model checkpoint, or other means that are appropriate to the research performed.
- While NeurIPS does not require releasing code, the conference does require all submissions to provide some reasonable avenue for reproducibility, which may depend on the nature of the contribution. For example
- (a) If the contribution is primarily a new algorithm, the paper should make it clear how to reproduce that algorithm.
- (b) If the contribution is primarily a new model architecture, the paper should describe the architecture clearly and fully.
- (c) If the contribution is a new model (e.g., a large language model), then there should either be a way to access this model for reproducing the results or a way to reproduce the model (e.g., with an open-source dataset or instructions for how to construct the dataset).
- (d) We recognize that reproducibility may be tricky in some cases, in which case authors are welcome to describe the particular way they provide for reproducibility. In the case of closed-source models, it may be that access to the model is limited in some way (e.g., to registered users), but it should be possible for other researchers to have some path to reproducing or verifying the results.

5. Open access to data and code

Question: Does the paper provide open access to the data and code, with sufficient instructions to faithfully reproduce the main experimental results, as described in supplemental material?

Answer: [Yes]

Justification: Once accepted, we will include a GitHub link, containing all the codes and pretrained models.

Guidelines:

- The answer NA means that paper does not include experiments requiring code.
- Please see the NeurIPS code and data submission guidelines (https://nips.cc/public/guides/CodeSubmissionPolicy) for more details.
- While we encourage the release of code and data, we understand that this might not be possible, so "No" is an acceptable answer. Papers cannot be rejected simply for not including code, unless this is central to the contribution (e.g., for a new open-source benchmark).
- The instructions should contain the exact command and environment needed to run to reproduce the results. See the NeurIPS code and data submission guidelines (https://nips.cc/public/guides/CodeSubmissionPolicy) for more details.
- The authors should provide instructions on data access and preparation, including how
 to access the raw data, preprocessed data, intermediate data, and generated data, etc.
- The authors should provide scripts to reproduce all experimental results for the new proposed method and baselines. If only a subset of experiments are reproducible, they should state which ones are omitted from the script and why.
- At submission time, to preserve anonymity, the authors should release anonymized versions (if applicable).
- Providing as much information as possible in supplemental material (appended to the paper) is recommended, but including URLs to data and code is permitted.

6. Experimental setting/details

Question: Does the paper specify all the training and test details (e.g., data splits, hyper-parameters, how they were chosen, type of optimizer, etc.) necessary to understand the results?

Answer: [Yes]

Justification: We have stated the settings clearly in the experiments section.

Guidelines:

- The answer NA means that the paper does not include experiments.
- The experimental setting should be presented in the core of the paper to a level of detail that is necessary to appreciate the results and make sense of them.
- The full details can be provided either with the code, in appendix, or as supplemental material.

7. Experiment statistical significance

Question: Does the paper report error bars suitably and correctly defined or other appropriate information about the statistical significance of the experiments?

Answer: [NA]

Justification: Error bars are not suitable for this paper. Instead, we have reported detailed quantitive values by different methods on a large dataset.

- The answer NA means that the paper does not include experiments.
- The authors should answer "Yes" if the results are accompanied by error bars, confidence intervals, or statistical significance tests, at least for the experiments that support the main claims of the paper.
- The factors of variability that the error bars are capturing should be clearly stated (for example, train/test split, initialization, random drawing of some parameter, or overall run with given experimental conditions).
- The method for calculating the error bars should be explained (closed form formula, call to a library function, bootstrap, etc.)
- The assumptions made should be given (e.g., Normally distributed errors).

- It should be clear whether the error bar is the standard deviation or the standard error
 of the mean.
- It is OK to report 1-sigma error bars, but one should state it. The authors should preferably report a 2-sigma error bar than state that they have a 96% CI, if the hypothesis of Normality of errors is not verified.
- For asymmetric distributions, the authors should be careful not to show in tables or figures symmetric error bars that would yield results that are out of range (e.g. negative error rates).
- If error bars are reported in tables or plots, The authors should explain in the text how they were calculated and reference the corresponding figures or tables in the text.

8. Experiments compute resources

Question: For each experiment, does the paper provide sufficient information on the computer resources (type of compute workers, memory, time of execution) needed to reproduce the experiments?

Answer: [Yes]

Justification: We have reported these informations.

Guidelines:

- The answer NA means that the paper does not include experiments.
- The paper should indicate the type of compute workers CPU or GPU, internal cluster, or cloud provider, including relevant memory and storage.
- The paper should provide the amount of compute required for each of the individual experimental runs as well as estimate the total compute.
- The paper should disclose whether the full research project required more compute than the experiments reported in the paper (e.g., preliminary or failed experiments that didn't make it into the paper).

9. Code of ethics

Question: Does the research conducted in the paper conform, in every respect, with the NeurIPS Code of Ethics https://neurips.cc/public/EthicsGuidelines?

Answer: [Yes]

Justification: We have carefully reviewed the NeurIPS Code of Ethics.

Guidelines:

- The answer NA means that the authors have not reviewed the NeurIPS Code of Ethics.
- If the authors answer No, they should explain the special circumstances that require a
 deviation from the Code of Ethics.
- The authors should make sure to preserve anonymity (e.g., if there is a special consideration due to laws or regulations in their jurisdiction).

10. Broader impacts

Question: Does the paper discuss both potential positive societal impacts and negative societal impacts of the work performed?

Answer: [NA]

Justification: This paper is not related to any potential positive societal impacts and negative societal impacts.

- The answer NA means that there is no societal impact of the work performed.
- If the authors answer NA or No, they should explain why their work has no societal impact or why the paper does not address societal impact.
- Examples of negative societal impacts include potential malicious or unintended uses (e.g., disinformation, generating fake profiles, surveillance), fairness considerations (e.g., deployment of technologies that could make decisions that unfairly impact specific groups), privacy considerations, and security considerations.

- The conference expects that many papers will be foundational research and not tied to particular applications, let alone deployments. However, if there is a direct path to any negative applications, the authors should point it out. For example, it is legitimate to point out that an improvement in the quality of generative models could be used to generate deepfakes for disinformation. On the other hand, it is not needed to point out that a generic algorithm for optimizing neural networks could enable people to train models that generate Deepfakes faster.
- The authors should consider possible harms that could arise when the technology is being used as intended and functioning correctly, harms that could arise when the technology is being used as intended but gives incorrect results, and harms following from (intentional or unintentional) misuse of the technology.
- If there are negative societal impacts, the authors could also discuss possible mitigation strategies (e.g., gated release of models, providing defenses in addition to attacks, mechanisms for monitoring misuse, mechanisms to monitor how a system learns from feedback over time, improving the efficiency and accessibility of ML).

11. Safeguards

Question: Does the paper describe safeguards that have been put in place for responsible release of data or models that have a high risk for misuse (e.g., pretrained language models, image generators, or scraped datasets)?

Answer: [Yes]

Justification: This paper poses no such risks.

Guidelines:

- The answer NA means that the paper poses no such risks.
- Released models that have a high risk for misuse or dual-use should be released with necessary safeguards to allow for controlled use of the model, for example by requiring that users adhere to usage guidelines or restrictions to access the model or implementing safety filters.
- Datasets that have been scraped from the Internet could pose safety risks. The authors should describe how they avoided releasing unsafe images.
- We recognize that providing effective safeguards is challenging, and many papers do not require this, but we encourage authors to take this into account and make a best faith effort.

12. Licenses for existing assets

Question: Are the creators or original owners of assets (e.g., code, data, models), used in the paper, properly credited and are the license and terms of use explicitly mentioned and properly respected?

Answer: [Yes]

Justification: All datasets are properly cited in the paper.

- The answer NA means that the paper does not use existing assets.
- The authors should cite the original paper that produced the code package or dataset.
- The authors should state which version of the asset is used and, if possible, include a URL.
- The name of the license (e.g., CC-BY 4.0) should be included for each asset.
- For scraped data from a particular source (e.g., website), the copyright and terms of service of that source should be provided.
- If assets are released, the license, copyright information, and terms of use in the package should be provided. For popular datasets, paperswithcode.com/datasets has curated licenses for some datasets. Their licensing guide can help determine the license of a dataset.
- For existing datasets that are re-packaged, both the original license and the license of the derived asset (if it has changed) should be provided.

• If this information is not available online, the authors are encouraged to reach out to the asset's creators.

13. New assets

Question: Are new assets introduced in the paper well documented and is the documentation provided alongside the assets?

Answer: [Yes]

Justification: The paper does not release new assets.

Guidelines:

- The answer NA means that the paper does not release new assets.
- · Researchers should communicate the details of the dataset/code/model as part of their submissions via structured templates. This includes details about training, license, limitations, etc.
- The paper should discuss whether and how consent was obtained from people whose asset is used.
- At submission time, remember to anonymize your assets (if applicable). You can either create an anonymized URL or include an anonymized zip file.

14. Crowdsourcing and research with human subjects

Question: For crowdsourcing experiments and research with human subjects, does the paper include the full text of instructions given to participants and screenshots, if applicable, as well as details about compensation (if any)?

Answer: [Yes]

Justification: The paper does not involve crowdsourcing nor research with human subjects. Guidelines:

- The answer NA means that the paper does not involve crowdsourcing nor research with human subjects.
- Including this information in the supplemental material is fine, but if the main contribution of the paper involves human subjects, then as much detail as possible should be included in the main paper.
- According to the NeurIPS Code of Ethics, workers involved in data collection, curation, or other labor should be paid at least the minimum wage in the country of the data collector.

15. Institutional review board (IRB) approvals or equivalent for research with human subjects

Question: Does the paper describe potential risks incurred by study participants, whether such risks were disclosed to the subjects, and whether Institutional Review Board (IRB) approvals (or an equivalent approval/review based on the requirements of your country or institution) were obtained?

Answer: [NA]

Justification: The paper does not involve crowdsourcing nor research with human subjects. Guidelines:

- The answer NA means that the paper does not involve crowdsourcing nor research with human subjects.
- Depending on the country in which research is conducted, IRB approval (or equivalent) may be required for any human subjects research. If you obtained IRB approval, you should clearly state this in the paper.
- We recognize that the procedures for this may vary significantly between institutions and locations, and we expect authors to adhere to the NeurIPS Code of Ethics and the guidelines for their institution.
- · For initial submissions, do not include any information that would break anonymity (if applicable), such as the institution conducting the review.

16. Declaration of LLM usage

Question: Does the paper describe the usage of LLMs if it is an important, original, or non-standard component of the core methods in this research? Note that if the LLM is used only for writing, editing, or formatting purposes and does not impact the core methodology, scientific rigorousness, or originality of the research, declaration is not required.

Answer: [NA]

Justification: The core method development in this research does not involve LLMs as any important, original, or non-standard components.

- The answer NA means that the core method development in this research does not involve LLMs as any important, original, or non-standard components.
- Please refer to our LLM policy (https://neurips.cc/Conferences/2025/LLM) for what should or should not be described.

A Technical Appendices and Supplementary Material

Contents

1	Introduction	2
2	CoCo denoisers	4
	2.1 Cocoercive denoisers	4
	2.2 Conservative denoisers	5
	2.3 Characterization on CoCo denoisers	6
3	Training strategy	6
4	PnP methods with CoCo denoisers	7
5	Experiments	8
6	Conclusion and Limitation	10
A	Technical Appendices and Supplementary Material	23
	A.1 Proof of Lemma 2.1	24
	A.2 Characterizations on the denoiser	24
	A.3 More general characterization on the CoCo denoiser	24
	A.4 Proof of Theorem 2.2	25
	A.5 Calculation for $\ (2\gammaJ-I)\ _*$ and $\ J-J^T\ _*$ $\ \ldots$	28
	A.6 Proof of Theorem 4.1	29
	A.7 Proof of Theorem 4.4	32
	A.8 Proximal operator on the fidelity for each task	33
	A.9 Detailed Deconvolution results on each kernel	33
	A.10 Single photon imaging	34
	A.11 Ablation study on γ and t in CoCo-PnP	34
	A.12 Low-dose CT reconstruction	34
	A.13 Poisson denoising results	35
	A.14 Computational cost	35
	A.15 Performances under extreme conditions	36
	A.16 Ablation study on the parameters α_1 and α_2	36
	A.17 Blind Deblur Results	37
	A.18 Blind Denoise Results	38

A.1 Proof of Lemma 2.1

In order to prove Lemma 2.1, we will mainly use Proposition 3.1 by [6]:

Proposition A.1 (Proposition 3.1 by [6]). Let C be a nonempty open convex subset of V, let \mathcal{B} be a real Banach space, and let $D: C \to \mathcal{B}$ be continuously Fréchet differentiable on C. Then D is non-expansive if and only if $\|J(x)\|_* \le 1$, $\forall x \in C, J(x) := \nabla D(x)$.

Now we prove Lemma 2.1.

Proof. In Lemma 2.1, we let $C=\mathcal{B}=V$, thus C is open convex, and \mathcal{B} is a real Banach space. In order to prove Lemma 2.1, we only need to prove that D is γ -cocoercive ($\gamma \in [0,\infty)$), if and only if $\forall x,y \in V$

$$\|(2\gamma D - I) \circ (x) - (2\gamma D - I) \circ (y)\| \le \|x - y\|. \tag{25}$$

Note that (25) is equivalent to

$$4\gamma^{2} \| D(x) - D(y) \|^{2} + \|x - y\|^{2} - 4\gamma \langle x - y, D(x) - D(y) \rangle \le \|x - y\|^{2}, \tag{26}$$

and equivalent to

$$\gamma \| D(x) - D(y) \|^2 \le \langle x - y, D(x) - D(y) \rangle, \tag{27}$$

which means D is γ -cocoercive.

A.2 Characterizations on the denoiser

The first characterization of proximal operators of convex, closed, and proper functions is due to Moreau's theorem [47].

Theorem A.2 ([47]). A map D: $V \to V$ is a proximal operator of a proper, closed, convex function $F: V \to \mathbb{R} \cup \{+\infty\}$, if and only if the it holds that:

- there exists a convex, closed function ψ such that $D(x) \in \partial \psi(x), \forall x \in V$;
- D is nonexpansive, i.e.,

$$\|D(x) - D(y)\| \le \|x - y\|, \forall x, y \in V.$$
 (28)

[22] generalized Moreau's theorem to the proximal operators of potentially nonconvex functions.

Theorem A.3 ([22]). Let $D: V \to V$ and L > 0. The following are equivalent:

- there is $F: V \to \mathbb{R} \cup \{+\infty\}$ such that $D(x) \in \operatorname{Prox}_F(x), \forall x \in V$, and $x \mapsto F(x) + (1 \frac{1}{L}) \frac{\|x\|^2}{2}$ is closed and convex;
- D is L-Lipschitz, and that there exists a closed, convex function ψ such that $D(x) \in \partial \psi(x), \forall x \in V$.

When $D \in \mathcal{C}^1[V]$, Gribonval and Nikolova also provided the following characterization.

Theorem A.4 ([22]). Let D: $V \to V$, and D $\in \mathcal{C}^1[V]$. The following properties are equivalent:

- D is a proximal operator of a function $F: V \to \mathbb{R} \cup \{+\infty\}$;
- there exists a convex $C^2[V]$ function ψ such that $D(x) = \nabla \psi(x), \forall x \in V$;
- the differential $J(x) = \nabla D(x)$ is symmetric positive semi-definite for all $x \in V$.

A.3 More general characterization on the CoCo denoiser

The following theorem is a tight use of Theorem A.4.

Theorem A.5. Let $D_{\sigma} \in \mathcal{C}^1[V]$. $\beta = \frac{1}{\sigma^2}$. D_{σ} satisfies that:

- D_{σ} is conservative;
- D_{σ} is γ -cocoercive with $\gamma \in (0, \infty)$.

Then, there exists a function $F: V \to \overline{\mathbb{R}}$, such that F is r-weakly convex, where $r = \beta(1 - \gamma)$, and that $D_{\sigma}(x) \in \operatorname{Prox}_{\frac{F}{\alpha}}(x), \forall x \in V$.

Note that here is a little abuse of notation here: when $\gamma > 1$, r < 0. "r-weakly convexity with a negative r" actually means "(-r)-strongly convexity".

Proof. When D_{σ} is γ -cocoercive with $\gamma>0$, by Lemma 2.1, $\forall x\in V, \|2\gamma J(x)-I\|_*\leq 1$. Therefore, J(x) is positive semi-definite for any $x\in V$. Since D_{σ} is conservative, it has no Hamiltonian part, $J(x)=J^{T}(x), \forall x\in V$. Therefore, J(x) is symmetric semi-positive for any $x\in V$. By Poincaré's lemma (see Theorem 6.6.3 in [20]), there exists a convex $\mathcal{C}^{2}[V]$ function ψ such that $D_{\sigma}(x)=\nabla\psi(x), \forall x\in V$.

By Theorem A.4, there exists a function $F:V\to \bar{\mathbb{R}}$, such that $D_{\sigma}\in \operatorname{Prox}_{\frac{F}{\beta}}$, where we let $\beta=\frac{1}{\sigma^2}$ for convenience. Now we prove that F is weakly convex. Recall the resolvent form of a proximal operator: $\operatorname{Prox}_{\frac{F}{\beta}}=(\mathrm{I}+\frac{1}{\beta}\partial F)^{-1}$. Given any $x,y\in V$, choose arbitrary $u,v\in V$, $u=D_{\sigma}(x)\in (\mathrm{I}+\frac{1}{\beta}\partial F)^{-1}(x), v=D_{\sigma}(y)\in (\mathrm{I}+\frac{1}{\beta}\partial F)^{-1}(y)$, then

$$\beta(x-u) \in \partial F(u), \beta(y-v) \in \partial F(v).$$
 (29)

Since D_{σ} is γ -cocoercive, by definition 5,

$$\langle x - y, D_{\sigma}(x) - D_{\sigma}(y) \rangle \ge \gamma \|D_{\sigma}(x) - D_{\sigma}(y)\|^2. \tag{30}$$

By substituting u, v in (30), we have

$$\langle x - y, u - v \rangle \ge \gamma \|u - v\|^{2}$$

$$\langle (x - u) - (y - v) + (u - v), u - v \rangle \ge \gamma \|u - v\|^{2}$$

$$\langle \beta(x - u) - \beta(y - v) + \beta(u - v), u - v \rangle \ge \beta \gamma \|u - v\|^{2}$$

$$\langle \beta(x - u) - \beta(y - v), u - v \rangle \ge \beta(\gamma - 1) \|u - v\|^{2}$$

$$\langle \beta(x - u) - \beta(y - v), u - v \rangle + \beta(1 - \gamma) \|u - v\|^{2} \ge 0.$$
(31)

Recall (29), we know that F is r-weakly convex with $r = \beta(1 - \gamma)$.

A.4 Proof of Theorem 2.2

Please note that, when $\gamma \geq 1$, D_{σ} is firmly non-expansive and conservative, and therefore is a proximal operator of some convex function. In this case, r(t) could be negative: the "negative weakly convexity" actually means convexity. Since a convex implicit prior function F is out of interest in this paper, Theorem 2.2 focuses on the weakly convex case, that is, $\gamma \in (0,1)$.

Proof. Since D_{σ} is γ -cocoercive with $\gamma > 0$, D_{σ}^{t} is naturally $\frac{\gamma}{t + (1-t)\gamma}$ -cocoercive: $\forall x, y \in V$, we have

$$\langle D_{\sigma}(x) - D_{\sigma}(y), x - y \rangle \geq \gamma \| D_{\sigma}(x) - D_{\sigma}(y) \|^{2}
\langle \frac{1}{t} (D_{\sigma}^{t} - (1 - t) I) \circ (x) - \frac{1}{t} (D_{\sigma}^{t} - (1 - t) I) \circ (y), x - y \rangle
\geq \gamma \| \frac{1}{t} (D_{\sigma}^{t} - (1 - t) I) \circ (x) - \frac{1}{t} (D_{\sigma}^{t} - (1 - t) I) \circ (y) \|^{2}
t \langle D_{\sigma}^{t}(x) - D_{\sigma}^{t}(y), x - y \rangle - t (1 - t) \|x - y\|^{2} \geq \gamma \| D_{\sigma}^{t}(x) - D_{\sigma}^{t}(y) - (1 - t)(x - y) \|^{2}.$$
(32)

Denote $a = D_{\sigma}^{t}(x) - D_{\sigma}^{t}(y)$, b = x - y for convenience. Then we have

$$t\langle a,b\rangle - t(1-t)\|b\|^2 \ge \gamma \|a\|^2 - 2\gamma (1-t)\langle a,b\rangle + \gamma (1-t)^2 \|b\|^2, (t+2\gamma(1-t))\langle a,b\rangle \ge \gamma \|a\|^2 + (t(1-t)+\gamma(1-t)^2)\|b\|^2.$$
(33)

Now note that

$$\langle a, b \rangle = t \langle \mathcal{D}_{\sigma}(x) - \mathcal{D}_{\sigma}(y), x - y \rangle + (1 - t) \|x - y\|^2. \tag{34}$$

Since D_{σ} is γ -cocoercive with $\gamma > 0$, we know that D_{σ} is $\frac{1}{\gamma}$ -Lipschitz. Therefore, by Cauchy-Schwarz inequality,

$$\langle \mathcal{D}_{\sigma}(x) - \mathcal{D}_{\sigma}(y), x - y \rangle \le \frac{1}{\gamma} ||x - y||^2.$$
 (35)

That is,

$$\begin{array}{ll} \langle a, b \rangle & \leq \left(\frac{t}{\gamma} + 1 - t\right) \|b\|^2, \\
\gamma(1 - t)\langle a, b \rangle & \leq t(1 - t)\|b\|^2 + \gamma(1 - t)^2\|b\|^2.
\end{array} (36)$$

By substituting (36) into (33), we have

$$(t + \gamma(1 - t))\langle a, b \rangle \ge \gamma \|a\|^2,$$

$$\langle a, b \rangle \ge \frac{\gamma}{t + \gamma(1 - t)} \|a\|^2,$$
(37)

which means that D_{σ}^{t} is $\frac{\gamma}{t+\gamma(1-t)}$ -cocoercive. Since D_{σ} is conservative, D_{σ}^{t} is also conservative. By Theorem A.5, we know that there exists a r-weakly convex function $F: V \to \overline{\mathbb{R}}$, where

$$r = r(t) = \beta \left(1 - \frac{\gamma}{t + \gamma(1 - t)} \right) = \beta \frac{t - \gamma t}{t + \gamma - \gamma t},$$

such that $D_{\sigma}^t \in \operatorname{Prox}_{\frac{F}{\beta}}$.

Now we prove that ∂F is L-Lipschitz. We consider two cases seperately. Case 1: $t \geq \frac{1-2\gamma}{2-2\gamma}$ and $t \in [0,1)$.

In this case, we need to prove that ∂F is $L(t)=\beta\frac{t}{1-t}$ Lipschitz. Given $\forall x,y\in V$, choose arbitrary u,v, such that, $u=\mathrm{D}_{\sigma}^t(x)\in (\mathrm{I}+\frac{1}{\beta}\partial F)^{-1}(x), v=\mathrm{D}_{\sigma}^t(y)\in (\mathrm{I}+\frac{1}{\beta}\partial F)^{-1}(y)$, then

$$\beta(x-u) \in \partial F(u), \beta(y-v) \in \partial F(v).$$
 (38)

Note that a=u-v, b=x-y. In order to prove ∂F is L(t)-Lipschitz, we need to prove

$$\|\beta(x-u) - \beta(y-v)\|^{2} \leq L^{2}(t)\|u-v\|^{2} = \beta^{2} \frac{t^{2}}{(1-t)^{2}} \|u-v\|^{2},$$

$$\|\beta(b-a)\|^{2} \leq \beta^{2} \frac{t^{2}}{(1-t)^{2}} \|a\|^{2},$$

$$\|b-a\|^{2} \leq \frac{t^{2}}{(1-t)^{2}} \|a\|^{2}.$$
(39)

Since
$$a = u - v = D_{\sigma}^{t}(x) - D_{\sigma}^{t}(y) = t(D_{\sigma}(x) - D_{\sigma}(y)) + (1 - t)(x - y), b = x - y$$
, we have
$$a - b = t(D_{\sigma}(x) - D_{\sigma}(y)) - t(x - y). \tag{40}$$

Now we only need to prove

$$t^{2} \| D_{\sigma}(x) - D_{\sigma}(y) \|^{2} - 2t^{2} \langle D_{\sigma}(x) - D_{\sigma}(y), x - y \rangle + t^{2} \|x - y\|^{2}$$

$$\leq \frac{t^{2}}{(1-t)^{2}} \left(t^{2} \| D_{\sigma}(x) - D_{\sigma}(y) \|^{2} + 2t(1-t) \langle D_{\sigma}(x) - D_{\sigma}(y), x - y \rangle + (1-t)^{2} \|x - y\|^{2} \right),$$
(41)

which is equivalent to prove

$$\frac{1-2t}{2-2t} \| D_{\sigma}(x) - D_{\sigma}(y) \|^2 \le \langle D_{\sigma}(x) - D_{\sigma}(y), x - y \rangle.$$

$$(42)$$

Since $t \ge \frac{1-2\gamma}{2-2\gamma}$, we have that

$$\frac{1-2t}{2-2t} \le \frac{1-2\frac{1-2\gamma}{2-2\gamma}}{2-2\frac{1-2\gamma}{2-2\gamma}} = \frac{2-2\gamma-2(1-2\gamma)}{2(2-2\gamma)-2(1-2\gamma)} = \frac{2\gamma}{2} = \gamma. \tag{43}$$

We already have

$$\gamma \| D_{\sigma}(x) - D_{\sigma}(y) \|^{2} \le \langle D_{\sigma}(x) - D_{\sigma}(y), x - y \rangle.$$
(44)

Thus,

$$\frac{1-2t}{2-2t} \| \operatorname{D}_{\sigma}(x) - \operatorname{D}_{\sigma}(y) \|^{2} \le \gamma \| \operatorname{D}_{\sigma}(x) - \operatorname{D}_{\sigma}(y) \|^{2} \le \langle \operatorname{D}_{\sigma}(x) - \operatorname{D}_{\sigma}(y), x - y \rangle. \tag{45}$$

Case 2: $t \leq \frac{1-2\gamma}{2-2\gamma}$ and $t \in [0,1)$.

In this case, we need to prove that ∂F is $L(t)=r(t)=\beta\frac{t-t\gamma}{t+\gamma-t\gamma}$ Lipschitz. Similarly in (39), we need to prove

$$\|\beta(x-u) - \beta(y-v)\|^{2} \leq L^{2}(t)\|u-v\|^{2} = \beta^{2} \frac{t^{2}(1-\gamma)^{2}}{(t+\gamma-t\gamma)^{2}} \|u-v\|^{2},$$

$$\|b-a\|^{2} \leq \frac{t^{2}(1-\gamma)^{2}}{(t+\gamma-t\gamma)^{2}} \|a\|^{2}.$$
(46)

Since
$$a = u - v = D_{\sigma}^{t}(x) - D_{\sigma}^{t}(y) = t(D_{\sigma}(x) - D_{\sigma}(y)) + (1 - t)(x - y), b = x - y$$
, we have
$$a - b = t(D_{\sigma}(x) - D_{\sigma}(y)) - t(x - y). \tag{47}$$

Now we only need to prove

$$t^{2} \| D_{\sigma}(x) - D_{\sigma}(y) \|^{2} - 2t^{2} \langle D_{\sigma}(x) - D_{\sigma}(y), x - y \rangle + t^{2} \|x - y\|^{2}$$

$$\leq \frac{t^{2} (1 - \gamma)^{2}}{(t + \gamma - t\gamma)^{2}} \left(t^{2} \| D_{\sigma}(x) - D_{\sigma}(y) \|^{2} + 2t (1 - t) \langle D_{\sigma}(x) - D_{\sigma}(y), x - y \rangle + (1 - t)^{2} \|x - y\|^{2} \right). \tag{48}$$

When t=0, it holds naturally. When $t\in(0,1)$, and $t\leq\frac{1-2\gamma}{2-2\gamma}$, it is equivalent to prove

$$\| D_{\sigma}(x) - D_{\sigma}(y) \|^{2} - 2\langle D_{\sigma}(x) - D_{\sigma}(y), x - y \rangle + \|x - y\|^{2} \le \frac{(1 - \gamma)^{2}}{(t + \gamma - t\gamma)^{2}} \left(t^{2} \| D_{\sigma}(x) - D_{\sigma}(y) \|^{2} + 2t(1 - t)\langle D_{\sigma}(x) - D_{\sigma}(y), x - y \rangle + (1 - t)^{2} \|x - y\|^{2} \right),$$
(49)

which is equivalent to prove

$$(t + \gamma - t\gamma)^{2} \left[\| D_{\sigma}(x) - D_{\sigma}(y) \|^{2} - 2\langle D_{\sigma}(x) - D_{\sigma}(y), x - y \rangle + \|x - y\|^{2} \right]$$

$$\leq (1 - \gamma)^{2} \left[t^{2} \| D_{\sigma}(x) - D_{\sigma}(y) \|^{2} + 2t(1 - t)\langle D_{\sigma}(x) - D_{\sigma}(y), x - y \rangle + (1 - t)^{2} \|x - y\|^{2} \right],$$
(50)

that is to prove

$$\begin{aligned}
& \left[(t + \gamma - t\gamma)^2 - t^2 (1 - \gamma)^2 \right] \| D_{\sigma}(x) - D_{\sigma}(y) \|^2 \\
& - \left[2(t + \gamma - t\gamma)^2 + 2t(1 - t)(1 - \gamma)^2 \right] \langle D_{\sigma}(x) - D_{\sigma}(y), x - y \rangle \\
& \leq \left[(1 - t)^2 (1 - \gamma)^2 - (t + \gamma - t\gamma)^2 \right] \|x - y\|^2.
\end{aligned} (51)$$

Now we check each coefficient, and estimate each term carefully. For the coefficient of $\|D_{\sigma}(x) - D_{\sigma}(y)\|^2$, we have

$$(t + \gamma - t\gamma)^2 - t^2(1 - \gamma)^2 = 2\gamma(1 - \gamma)t + \gamma^2 > 0$$
(52)

For the coefficient of $\langle D_{\sigma}(x) - D_{\sigma}(y), x - y \rangle$, it is obviously non-positive. Besides, we have that

of
$$\langle D_{\sigma}(x) - D_{\sigma}(y), x - y \rangle$$
, it is obviously hori-positive. Besides, we have that
$$- \left[2(t + \gamma - t\gamma)^2 + 2t(1 - t)(1 - \gamma)^2 \right]$$

$$= -2 \left[(1 - \gamma)^2 t^2 + 2\gamma(1 - \gamma)t + \gamma^2 + (t - t^2)(1 - \gamma)^2 \right]$$

$$= -(2 - 2\gamma^2)t - 2\gamma^2.$$
(53)

Since D_{σ} is γ -cocoercive, we have that

$$\left[-(2-2\gamma^2)t-2\gamma^2\right]\langle \mathcal{D}_{\sigma}(x)-\mathcal{D}_{\sigma}(y),x-y\rangle \leq \left[-\gamma(2-2\gamma^2)t-2\gamma^3\right]\|\mathcal{D}_{\sigma}(x)-\mathcal{D}_{\sigma}(y)\|^2. \tag{54}$$

For the coefficient of $||x-y||^2$, note that when $\gamma \in (0,1)$, $t \in [0,1)$, and $t \leq \frac{1-2\gamma}{2-2\gamma}$, we have

$$(1-t)^2(1-\gamma)^2 - (t+\gamma-t\gamma)^2 = (2\gamma-2)t - 2\gamma + 1 \ge (2\gamma-2)\frac{1-2\gamma}{2-2\gamma} - 2\gamma + 1 \ge 0.$$
 (55)

Combining (52)-(55), to prove (51), we only need to prove that

$$\left[2\gamma(1-\gamma)t + \gamma^{2} - \gamma(2-2\gamma^{2})t - 2\gamma^{3}\right] \| D_{\sigma}(x) - D_{\sigma}(y) \|^{2} \leq \left[(2\gamma-2)t - 2\gamma+1\right] \|x-y\|^{2}
\iff \left[(2\gamma^{3} - 2\gamma^{2})t + \gamma^{2} - 2\gamma^{3}\right] \| D_{\sigma}(x) - D_{\sigma}(y) \|^{2} \leq \left[(2\gamma-2)t - 2\gamma+1\right] \|x-y\|^{2}. \tag{56}$$

Since D_{σ} is $\frac{1}{2}$ -Lipschitz, we only need to prove that

$$\frac{1}{\gamma^2} \left[(2\gamma^3 - 2\gamma^2)t + \gamma^2 - 2\gamma^3 \right] \le (2\gamma - 2)t - 2\gamma + 1$$

$$(2\gamma - 2)t + 1 - 2\gamma \le (2\gamma - 2)t - 2\gamma + 1.$$
(57)

This completes the proof.

Please note that any Lipschitz operator must be single-valued. Thus, there is actually only one element in $\partial F(x)$, given any $x \in V$.

A.5 Calculation for $\|(2\gamma J - I)\|_*$ and $\|J - J^T\|_*$

We mainly use the power iterative method [21] to calculate the spectral norm of a given operator A.

Algorithm 1 Power iterative method

$$\begin{aligned} & \text{Given } q^0 \text{ with } \|q^0\| = 1, A, N \\ & \textbf{for } n = 1 : N \textbf{ do} \\ & z^n = A \, q^{n-1} \\ & q^n = \frac{z^n}{\|z^n\|} \\ & \textbf{end for} \\ & \text{Return } \lambda^N = (q^N)^{\text{T}} \, \mathbf{A} \, q^N \end{aligned}$$

By Algorithm 1, we can compute the spectral norm of A. Note that in Algorithm 1, we need to calculate the matrix-vector product A q, given any $q \in V$.

Given a denoiser D_{σ} , $\forall x \in V$, $J(x) = \nabla D_{\sigma}(x)$ is the Jacobian matrix at the point x. To specify, let $x = [x_1, x_2, \dots, x_n]^T \in V = \mathbb{R}^n$, and $y = [y_1, y_2, \dots, y_n]^T = D_{\sigma}(x)$ be the output after D_{σ} . Then the Jacobian matrix $J(x^*)$ at a given point x^* is:

$$J(x^*) = \begin{bmatrix} \frac{\partial y_1}{\partial x_1} & \frac{\partial y_1}{\partial x_2} & \dots & \frac{\partial y_1}{\partial x_n} \\ \frac{\partial y_2}{\partial y_2} & \frac{\partial y_2}{\partial x_2} & \dots & \frac{\partial y_2}{\partial x_n} \\ \vdots & \vdots & \ddots & \vdots \\ \frac{\partial y_n}{\partial x_1} & \frac{\partial y_n}{\partial x_2} & \dots & \frac{\partial y_n}{\partial x_n} \end{bmatrix}_{x=x^*}$$

$$(58)$$

We start with $a = [a_1, a_2, \dots, a_n]^T = J^T(x)v$, where $v = [v_1, v_2, \dots, v_n]^T$ is any vector. By basic linear algebra, we know that

$$a_i = \sum_{i=1}^n \frac{\partial y_j}{\partial x_i} v_j, \ \forall i = 1, 2, \dots, n,$$

$$(59)$$

which implies

$$a = \mathbf{J}^{\mathrm{T}}(x)v = \frac{\partial \langle y, v \rangle}{\partial x}.$$
 (60)

The calculation of b = J(x)v is a bit more complex. We will use the so-called double back-propagation technique: since b = J(x)v, we have

$$b_k = \sum_{i=1}^n \frac{\partial y_k}{\partial x_i} v_i, \ \forall k = 1, 2, \dots, n.$$
 (61)

Now consider $w = [w_1, w_2, \dots, w_n]^T$. Let $t = J^T(x)w$. Thus $t_i = \sum_{j=1}^n \frac{\partial y_j}{\partial x_i} w_j$.

Let
$$z = \frac{\partial \langle t, v \rangle}{\partial w}$$
, then

$$z = \frac{\partial \langle t, v \rangle}{\partial w} = \frac{\partial}{\partial w} \left(\sum_{i=1}^{n} v_i \left(\sum_{j=1}^{n} \frac{\partial y_j}{\partial x_i} w_j \right) \right). \tag{62}$$

The kth element of z is:

$$z_k = \frac{\partial}{\partial w_k} \left(\sum_{i=1}^n v_i \left(\sum_{j=1}^n \frac{\partial y_j}{\partial x_i} w_j \right) \right) = \sum_{i=1}^n v_i \frac{\partial y_k}{\partial x_i}, \ \forall k = 1, 2, \dots, n.$$
 (63)

That is,

$$z = J(x)v = \frac{\partial \langle t, v \rangle}{\partial w} = \frac{\partial \langle \frac{\partial \langle y, w \rangle}{\partial x}, v \rangle}{\partial w}, \ \forall w \in \mathbb{R}^n.$$
 (64)

The AutoGrad toolbox in Pytorch [50] allows the calculation for $\frac{\partial \langle \cdot, \cdot \rangle}{\partial \cdot}$. The pseudo-codes in Pytorch can be:

```
# Calculate J(x)v
def _jacobian_vec(y, x, v):
    w = torch.ones_like(x, require_grad=True)
    t = torch.autograd.grad(y, x, w, create_graph=True)[0]
    return torch.autograd.grad(t, w, v, create_graph=True)[0]
# Calculate J^T(x)v
def _jacobian_transpose_vec(y, x, v):
```

return torch.autograd.grad(y, x, v, create_graph=True)[0]

By (60) and (64), one can calculate $\|(2\gamma J - I)\|_*$ and $\|J - J^T\|_*$ by Algorithm 1.

A.6 Proof of Theorem 4.1

We will make use of the Lyapunov function L_{β} for (19) according to [40, 68, 29]:

$$L_{\beta}(u, v, b) = F(v) + G(u; f) + \beta \langle b, u - v \rangle + \frac{\beta}{2} ||u - v||^{2}.$$
 (65)

We will first prove in part 1 that an important value for $L_{\beta}(u, v, b)$ is positive whenever $t \in (0, t_0)$, where t_0 is the positive root of the characteristic equation in (20). Then, we will prove in part 2 that L_{β} is non-increasing with the iteration number k. Finally, we will prove in part 3 that CoCo-ADMM iteration in (19) converges globally to a stationary point of (15).

Proof. Let $h(t)=(2-2\gamma)t^3+\gamma t^2+2\gamma t-\gamma$, where $\gamma\in(0,1)$. Note that h is obviously smooth, and $h(0)=-\gamma<0$, $h(\infty)=\infty$. Also note that when t>0,

$$h'(t) = (2 - 2\gamma)t^2 + 2\gamma t + 2\gamma > 0.$$
(66)

Therefore, there exists a unique $t_0 > 0$, such that $h(t_0) = 0$, h(t) > 0 if $t > t_0$, and h(t) < 0 if $t \in [0, t_0)$.

Part 1:

We consider a characteristic value for $L_{\beta}(u, v, b)$ in (65): $\frac{\beta}{2} - \frac{r}{2} - \frac{L^2}{\beta}$.

By Theorem 2.2, if $t \in [0,1)$ and $t \ge \frac{1-2\gamma}{2-2\gamma}$, we have that $r = \beta \frac{t-\gamma t}{t+\gamma-t\gamma}$ and $L = \beta \frac{t}{1-t}$. Thus we have

$$\frac{\beta}{2} - \frac{r}{2} - \frac{L^2}{\beta} = \frac{\beta}{2} - \frac{\beta(t - \gamma t)}{2(t + \gamma - t\gamma)} - \frac{\beta t^2}{(1 - t)^2}$$

$$= \frac{\beta}{2} \left(1 - \frac{t - \gamma t}{t + \gamma - t\gamma} - \frac{2t^2}{(1 - t)^2} \right)$$

$$= \frac{\beta}{2(t + \gamma - t\gamma)(1 - t)^2} \left(\gamma(1 - t)^2 - 2t^2(t + \gamma - t\gamma) \right)$$

$$= -\frac{\beta}{2(t + \gamma - t\gamma)(1 - t)^2} \left((2 - 2\gamma)t^3 + \gamma t^2 + 2\gamma t - \gamma \right).$$
(67)

When $0 < t < t_0$, where t_0 is the positive root of the characteristic equation in (20), $\frac{\beta}{2} - \frac{r}{2} - \frac{L^2}{\beta} > 0$ holds.

If $t \in [0,1)$ and $t \leq \frac{1-2\gamma}{2-2\gamma}$, we have that $L=r=\beta\frac{t-\gamma t}{t+\gamma-t\gamma}$. Note that in this case, $L=r \leq \beta\frac{t}{1-t}$. Thus,

$$\frac{\beta}{2} - \frac{r}{2} - \frac{L^2}{\beta}$$

$$\geq \frac{\beta}{2} - \frac{\beta(t - \gamma t)}{2(t + \gamma - t\gamma)} - \frac{\beta t^2}{(1 - t)^2}$$

$$= -\frac{\beta}{2(t + \gamma - t\gamma)(1 - t)^2} \left((2 - 2\gamma)t^3 + \gamma t^2 + 2\gamma t - \gamma \right).$$
(68)

Therefore, we also have that when $0 < t < t_0, \frac{\beta}{2} - \frac{r}{2} - \frac{L^2}{\beta} > 0$ holds.

Part 2:

Now we prove that $L_{\beta}(u^k, v^k, b^k)$ is non-increasing. Before that, we show two important formulas. For v^{k+1} , by the first-order optimal condition, we know that

$$\beta b^{k+1} = -\beta (v^{k+1} - u^{k+1} - b^k) \in \partial F(v^{k+1}). \tag{69}$$

Similarly, for u^{k+1} , we have

$$-\beta(u^{k+1} - v^k + b^k) \in \partial G(u^{k+1}; f). \tag{70}$$

In order to prove that $L_{\beta}(u^k, v^k, b^k)$ is non-increasing, we decompose $L_{\beta}(u^k, v^k, b^k) - L_{\beta}(u^{k+1}, v^{k+1}, b^{k+1})$ into two parts:

$$L_{\beta}(u^{k}, v^{k}, b^{k}) - L_{\beta}(u^{k+1}, v^{k+1}, b^{k+1}) = L_{\beta}(u^{k}, v^{k}, b^{k}) - L_{\beta}(u^{k+1}, v^{k}, b^{k}) + L_{\beta}(u^{k+1}, v^{k}, b^{k}) - L_{\beta}(u^{k+1}, v^{k+1}, b^{k+1}),$$
(71)

and estimate them separately as follows. By the convexity of G and the iteration form in (19), we have

$$L_{\beta}(u^{k}, v^{k}, b^{k}) - L_{\beta}(u^{k+1}, v^{k}, b^{k})$$

$$= G(u^{k}; f) - G(u^{k+1}; f) + \beta \langle b^{k}, u^{k} - u^{k+1} \rangle + \frac{\beta}{2} \| u^{k} - v^{k} \|^{2} - \frac{\beta}{2} \| u^{k+1} - v^{k} \|^{2}$$

$$= G(u^{k}; f) - G(u^{k+1}; f) - \langle -\beta(u^{k+1} - v^{k} + b^{k}), u^{k} - u^{k+1} \rangle + \beta \langle v^{k} - u^{k+1}, u^{k} - u^{k+1} \rangle$$

$$+ \frac{\beta}{2} \| u^{k} - v^{k} \|^{2} - \frac{\beta}{2} \| u^{k+1} - v^{k} \|^{2}$$

$$\geq 0 + \beta \langle v^{k} - u^{k+1}, u^{k} - u^{k+1} \rangle + \frac{\beta}{2} \langle u^{k} - u^{k+1}, u^{k} + u^{k+1} - 2v^{k} \rangle$$

$$= \beta \langle u^{k} - u^{k+1}, v^{k} - u^{k+1} - v^{k} + \frac{u^{k} + u^{k+1}}{2} \rangle$$

$$= \frac{\beta}{2} \| u^{k} - u^{k+1} \|^{2}.$$

$$(72)$$

By the r-weakly convexity of F, $\forall x,y \in V, f_y \in \partial F(y)$, we have:

$$F(x) - F(y) \ge \langle f_y, x - y \rangle - \frac{r}{2} ||x - y||^2.$$
 (73)

By the L-Lipschitz property of ∂F , $\forall x, y \in V$, $f_y \in \partial F(y)$, we have:

$$F(x) - F(y) \le \langle f_y, x - y \rangle + \frac{L}{2} ||x - y||^2.$$
 (74)

Combining (73) and (74), we can obtain that

$$L_{\beta}(u^{k+1}, v^k, b^k) - L_{\beta}(u^{k+1}, v^{k+1}, b^{k+1})$$

$$= F(v^k) - F(v^{k+1}) + \beta \langle b^k, u^{k+1} - v^k \rangle - \beta \langle b^{k+1}, u^{k+1} - v^{k+1} \rangle$$

$$+ \frac{\beta}{2} \|u^{k+1} - v^k\|^2 - \frac{\beta}{2} \|u^{k+1} - v^{k+1}\|^2$$

$$= F(v^k) - F(v^{k+1}) + \beta \langle b^k, u^{k+1} - v^k \rangle - \beta \langle b^k, u^{k+1} - v^{k+1} \rangle - \beta \langle u^{k+1} - v^{k+1}, u^{k+1} - v^{k+1} \rangle$$

$$+ \frac{\beta}{2} \|v^k - v^{k+1}\|^2 + \beta \langle u^{k+1} - v^{k+1}, v^{k+1} - v^k \rangle$$

$$= F(v^k) - F(v^{k+1}) + \beta \langle b^k, v^{k+1} - v^k \rangle - \beta \|u^{k+1} - v^{k+1}\|^2$$

$$+ \frac{\beta}{2} \|v^k - v^{k+1}\|^2 + \beta \langle u^{k+1} - v^{k+1}, v^{k+1} - v^k \rangle$$

$$= F(v^k) - F(v^{k+1}) - \langle \beta b^k, v^{k+1} - v^k \rangle - \beta \|u^{k+1} - v^{k+1}\|^2 + \frac{\beta}{2} \|v^k - v^{k+1}\|^2$$

$$+ \beta \langle u^{k+1} - v^{k+1}, v^{k+1} - v^k \rangle$$

$$\geq -\frac{r}{2} \|v^k - v^{k+1}\|^2 - \beta \|u^{k+1} - v^{k+1}\|^2 + \frac{\beta}{2} \|v^k - v^{k+1}\|^2$$

$$= \left(\frac{\beta}{2} - \frac{r}{2}\right) \|v^k - v^{k+1}\|^2 - \beta \|b^k - b^{k+1}\|^2$$

$$\geq \left(\frac{\beta}{2} - \frac{r}{2}\right) \|v^k - v^{k+1}\|^2 - \frac{L^2}{\beta} \|v^k - v^{k+1}\|^2$$

$$= \left(\frac{\beta}{2} - \frac{r}{2}\right) \|v^k - v^{k+1}\|^2 - \frac{L^2}{\beta} \|v^k - v^{k+1}\|^2$$

$$= \left(\frac{\beta}{2} - \frac{r}{2} - \frac{L^2}{\beta}\right) \|v^k - v^{k+1}\|^2.$$
(75)

Note that the second '=' comes from the cosine rule, the first ' \geq ' follows from the r-weakly convexity of F as in (73), and the second ' \geq ' results from the L-Lipschitz of ∂F as in (74).

Combining (72) and (75), we get

$$L_{\beta}(u^{k}, v^{k}, b^{k}) - L_{\beta}(u^{k+1}, v^{k+1}, b^{k+1}) \ge \frac{\beta}{2} \|u^{k} - u^{k+1}\|^{2} + \left(\frac{\beta}{2} - \frac{r}{2} - \frac{L^{2}}{\beta}\right) \|v^{k} - v^{k+1}\|^{2} \ge 0,$$
(76)

that is, $L_{\beta}(u^k, v^k, b^k)$ is non-increasing.

Now we prove that $\{(u^k, v^k, b^k)\}$ is bounded. Note that F and G are coercive on V. As a result,

$$F(u^k) + G(u^k; f) > +\infty. (77)$$

Along with $\beta b^k \in \partial F(v^k)$ and the property that ∂F is L-Lipschitz, we arrive at

$$L_{\beta}(u^{k}, v^{k}, b^{k}) = F(v^{k}) + G(u^{k}; f) + \beta \langle b^{k}, u^{k} - v^{k} \rangle + \frac{\beta}{2} \|u^{k} - v^{k}\|^{2}$$

$$\geq F(u^{k}) + G(u^{k}; f) - \frac{L}{2} \|u^{k} - v^{k}\|^{2} + \frac{\beta}{2} \|u^{k} - v^{k}\|^{2}.$$
(78)

Note that $L = \frac{\beta t}{1-t}$, and that t < 0.5. Thus, $L < \beta$. Therefore,

$$F(u^{k}) + G(u^{k}; f) - \frac{L}{2} \|u^{k} - v^{k}\|^{2} + \frac{\beta}{2} \|u^{k} - v^{k}\|^{2}$$

$$= F(u^{k}) + G(u^{k}; f) + \frac{1}{2} (\beta - L) \|u^{k} - v^{k}\|^{2} \ge -\infty.$$
(79)

Since F(u) + G(u; f) is coercive on V, u^k, v^k, b^k are bounded.

Part 3:

Define q^{k+1} as follows:

$$q^{k+1} = [\beta(b^{k+1} - b^k + v^k - v^{k+1}), \beta(v^{k+1} - u^{k+1}), \beta(b^{k+1} - b^k)].$$
(80)

Define $\partial L_{\beta}(u, v, b) = [\partial_u L_{\beta}, \partial_v L_{\beta}, \partial_b L_{\beta}]$. By the formulas (69)-(70), we know that

$$q^{k+1} \in \partial L_{\beta}(u^{k+1}, v^{k+1}, b^{k+1}). \tag{81}$$

Note that

$$\|\beta(b^{k+1}-b^k+v^k-v^{k+1})\| \le \beta\|b^k-b^{k+1}\|+\beta\|v^k-v^{k+1}\| \le L\|v^k-v^{k+1}\|+\beta\|v^k-v^{k+1}\|, \tag{82}$$

and that

$$\|\beta(v^{k+1} - u^{k+1})\| = \beta\|b^k - b^{k+1}\| \le L\|v^k - v^{k+1}\|,\tag{83}$$

we arrive at

$$||q^{k+1}|| \le C||v^k - v^{k+1}||, \tag{84}$$

where

$$C = 3L + \beta. \tag{85}$$

Now we can finally prove Theorem 4.1. By Part 2, $\{(u^k, v^k, b^k)\}$ is bounded. So there is a sub-sequence $\{(u^{n_k}, v^{n_k}, b^{n_k})\}$ such that $(u^{n_k}, v^{n_k}, b^{n_k}) \to (u^*, v^*, b^*)$, when $n \to +\infty$. Since $L_\beta(u^k, v^k, b^k)$ is lower bounded and non-increasing, we have that $\|u^k - u^{k+1}\|, \|v^k - v^{k+1}\| \to 0$ as $k \to +\infty$. Besides, since $q^k \in \partial L_\beta(u^k, v^k, b^k)$ and $\|q^k\| \le C\|v^k - v^{k+1}\|$, we know that $\|q^k\| \to 0$, $\|q^{n_k}\| \to 0$. Thus, $0 \in \partial L_\beta(u^*, v^*, b^*)$, and (u^*, v^*, b^*) is a stationary point of L_β .

Since F, G is KL, we conclude that L_{β} is also KL. Then, by the proof of Theorem 2.9 in [2], $\{(u^{n_k}, v^{n_k}, b^{n_k})\}$ converges globally to (u^*, v^*, b^*) .

Since (u^*, v^*, b^*) is a stationary point of L_{β} , and as a result, $q^* = 0$, that is

$$q^* = [0, \beta(v^* - u^*), 0] = 0.$$
(86)

Therefore, $u^* = v^*$. By CoCo-ADMM iteration in (19), we know that

$$u^* = \operatorname{Prox}_{\frac{G}{\beta}}(u^* - b^*), u^* = \operatorname{D}_{\sigma}^t(u^* + b^*) \in \operatorname{Prox}_{\frac{G}{3}}(u^* + b^*).$$
(87)

Equivalently,

$$-\beta b^* \in \partial G(u^*; f), \beta b^* \in \partial F(u^*), \tag{88}$$

$$0 \in \partial F(u^*) + \partial G(u^*; f). \tag{89}$$

Therefore, u^* is a stationary point of (15).

A.7 Proof of Theorem 4.4

The convergence of PGD with weakly convex prior function has been extensively studied. For details, one can refer to [2, 27]. For example, [27] prove that

Theorem A.6 (Theorem 1 by [27]). Let F, H be proper, closed, bounded from below, and H is differentiable with L_H -Lipschitz gradient, and F is r-weakly convex. Then for $\tau < \max\{\frac{2}{L_H+r}, \frac{1}{L_H}\}$, the iterates

$$u^{k+1} \in \operatorname{Prox}_{\tau F} \circ (\mathbf{I} - \tau \nabla H)(u^k)$$
 (90)

verify

- $(F(u^k) + H(u^k))$ is non-increasing and converges.
- All cluster points of the sequence u^k are stationary points of F + H.
- If the sequence u^k is bounded and if F + H verifies the KL property at the cluster points of u^k , then u^k converges to a stationary point of F + H.

By Theorem A.6, we can prove Theorem 4.4.

Proof. Let F be the proper, closed, weakly convex prior function. Let $H = {}^{1}G$ be the Moreau envelope of G, that is

$$H(u) = {}^{1}G(u) := \min_{v} G(v) + \frac{1}{2} \|v - u\|^{2}.$$
(91)

Then ${}^{1}G$ is diffentiable:

$$\nabla^1 G = \mathbf{I} - \operatorname{Prox}_G. \tag{92}$$

Since G is proper, closed, and convex, its proximal operator is firmly non-expansive. Therefore, $\nabla^1 G$ is also firmly non-expansive, thus 1-Lipschitz. Since F and G is coercive and KL, $F+{}^1G$ is also coercive and KL. Therefore, u^k is bounded. By Theorem A.6, if $\frac{1}{\beta} < \max\{\frac{2}{1+r}, 1\}$, CoCo-PEGD converges to a stationary point of $F+{}^1G$.

A.8 Proximal operator on the fidelity for each task

When $K \neq I$, in general, there is no closed-form solution for $\operatorname{Prox}_{\frac{G}{\beta}}$. Given $f \in V$, we say $\hat{x} = \operatorname{Prox}_{\frac{G}{\beta}}(z)$, if

$$\hat{x} = \arg\min_{x} \lambda \langle \mathbf{1}, Kx - f \log Kx \rangle + \frac{\beta}{2} ||x - z||^2.$$
(93)

(93) is solved by ADMM with T iterations and $\rho > 0$ as follows:

$$x^{i+1} = (\beta + \rho K^{\top} K)^{-1} (\beta z + \rho K^{\top} (y^{i} - w^{i})),$$

$$y^{i+1} = \arg \min_{y} \lambda \langle \mathbf{1}, y - f \log y \rangle + \frac{\rho}{2} ||Kx^{i+1} - y + w^{i}||^{2},$$

$$w^{i+1} = w^{i} + Kx^{i+1} - y^{i+1}.$$
(94)

When K is a blur kernel, x-subproblem can be solved by the fast Fourier transformation as in [49]. When K = R is the Radon transform, one can calculate $(\beta + \rho K^{\mathrm{T}}K)^{-1}$ by the conjugate gradient method. There is a closed form solution for the y-subproblem by [34]:

$$y^{i+1} = \frac{z^i + \sqrt{(z^i)^2 + 4\rho\lambda f}}{2\rho},\tag{95}$$

where

$$z^{i} = \rho(Kx^{i+1} + \omega^{i}) - \lambda \mathbf{1}. \tag{96}$$

We initialize $x^0 = y^0 = z, w^0 = 0$, and output $\hat{x} = x^T$. We set T = 10 to ensure the convergence of the x-subproblem.

A.9 Detailed Deconvolution results on each kernel

See Tables 3-4.

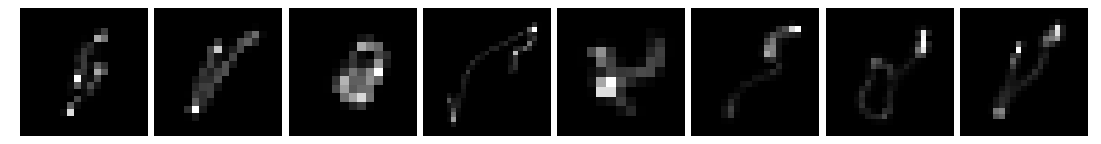


Figure 4: Eight blur kernels from [39].

Table 3: Average Deconvolution PSNR and SSIM performance by different methods on CBSD68 dataset with Poisson noise with peak value p = 100.

p=100	kernel1	kernel2	kernel3	kernel4	kernel5	kernel6	kernel7	kernel8	Average
DPIR	26.24	25.97	26.66	25.65	27.61	27.42	26.52	26.00	26.51
	0.7321	0.7209	0.7439	0.7016	0.7870	0.7780	0.7462	0.7257	0.7419
RMMO-DRS	25.60	25.39	26.07	25.19	26.92	26.59	26.06	25.67	25.94
	0.6895	0.6804	0.7057	0.6665	0.7426	0.7296	0.7089	0.6921	0.7019
Prox-DRS	25.32	25.03	25.82	24.80	26.75	26.39	25.94	25.40	25.68
	0.6546	0.6488	0.6842	0.6336	0.7256	0.7050	0.6924	0.6668	0.6764
DPS	23.40	23.23	24.19	22.86	24.74	24.06	23.60	23.10	23.65
DiffPIR	0.5941	0.5882	0.6303	0.5699	0.6550	0.6265	0.6039	0.5815	0.6062
	24.46	24.45	25.03	24.17	25.66	25.27	24.93	24.56	24.82
SNORE	0.6250	0.6251	0.6510	0.6085	0.6838	0.6664	0.6509	0.6325	0.6429
	25.75	25.99	26.56	25.70	27.13	26.85	26.55	26.09	26.33
PnPI-HOS	0.6985	0.6993	0.7202	0.6856	0.7485	0.7405	0.7249	0.7085	0.7158
	26.25	25.95	26.32	25.70	27.32	27.15	26.55	26.15	26.42
	0.7024	0.6930	0.7124	0.6797	0.7570	0.7466	0.7269	0.7084	0.7158
B-RED	23.89	23.55	24.09	23.33	25.04	24.61	24.33	23.88	24.09
	0.6206	0.6188	0.6537	0.5988	0.6824	0.6584	0.6434	0.6200	0.6370
CoCo-ADMM	26.66 0.7270	26.46 0.7183	26.93 0.7343	26.23 0.7075	27.78 0.7707	27.52 0.7630	26.96 0.7404	26.59 0.7254	26.89 0.7358

Table 4: Average Poisson deblurring PSNR and SSIM performance by different methods on CBSD68 dataset with Poisson noise with peak value p=50.

p=50	kernel1	kernel2	kernel3	kernel4	kernel5	kernel6	kernel7	kernel8	Average
DPIR	25.10	24.83	25.66	24.50	26.45	26.20	25.41	24.89	25.38
	0.6773	0.6656	0.6988	0.6480	0.7390	0.7261	0.6981	0.6752	0.6910
RMMO-DRS	24.86	24.73	25.39	24.51	25.84	25.52	25.12	24.83	25.10
	0.6439	0.6419	0.6690	0.6292	0.6826	0.6697	0.6549	0.6457	0.6546
Prox-DRS	24.89	24.69	25.45	24.43	26.14	25.81	25.36	24.92	25.21
	0.6363	0.6319	0.6676	0.6164	0.7024	0.6829	0.6714	0.6484	0.6572
DPS	22.92	22.76	23.72	22.34	24.13	23.48	22.98	22.49	23.10
	0.5724	0.5668	0.6088	0.5475	0.6266	0.5990	0.5758	0.5561	0.5816
DiffPIR	23.79	23.73	24.43	23.45	24.91	24.45	24.16	23.77	24.08
	0.5915	0.5894	0.6220	0.5744	0.6478	0.6263	0.6134	0.5941	0.6074
SNORE	24.57	25.06	25.80	24.75	25.78	25.34	25.34	25.01	25.21
	0.6522	0.6617	0.6893	0.6490	0.6967	0.6863	0.6749	0.6648	0.6719
PnPI-HQS	25.54	25.29	25.80	25.02	25.60	26.37	25.83	25.41	25.61
	0.6972	0.6705	0.6943	0.6563	0.7359	0.7231	0.7039	0.6837	0.6956
B-RED	23.49	23.41	23.86	22.99	24.69	24.49	23.86	23.46	23.78
	0.6083	0.6059	0.6436	0.5854	0.6692	0.6441	0.6264	0.6027	0.6232
CoCo-ADMM	27.74	25.57	26.16	25.32	26.89	26.52	26.09	25.67	26.00
	0.6906	0.6817	0.7072	0.6701	0.7412	0.7289	0.7098	0.6911	0.7026

A.10 Single photon imaging

We test the proposed methods in a low-light real-world scenario: single photon imaging task by a time-correlated single-photon avalanche diode (SPAD) camera [62]. In this task, a SPAD array is used to track periodic light pulses in flight, and each detector only recieves about 1 signal photon per pixel on average ($p \approx 1$). By the uncertainty principle [26, 56], since the momentum of the photons is known, the position of the photons cannot be accurately recorded. Therefore, the arrival time of each photon in the SPAD array is a random variable, and can be modelled by a Poisson process. By the filtered histogram method, a reflectivity image⁵ is obtained, see Fig. 3 (a).

We compare the visual denoising performance on Fig. 3 (a) by some state-of-the-art Poisson noise removal methods: Photon TV using a TV prior specialized for this problem [62]; BM3D-VST, a BM3D method with variance stabilization transform designed for Poisson noises [3]; DnCNN [74] trained as a Poisson denoiser; VDIR, a variational inference network [63]; VBDNet, a variational bayesian deep network for blind poisson denoising [41]. We also compare three PnP methods, DPIR, RMMO-DRS, and PnPI-HQS, as introduced before.

We show the visual results in Fig. 3. It can be seen in Figs. 3 (b)-(c) that, non-deep methods provide blurred results with unclear edges. End-to-end deep learning methods provide over-smoothed results, and cannot restore the fine details in the flower, see Figs. 3 (d)-(f). Compared with other PnP methods, CoCo methods can recover the fine textures in the flower, as well as the sharp edges in the equation, see Figs. 3 (g)-(k). Since there is no reference image in this real-world scenario, we only report the relative error curves to validate the convergence in Fig. 3 (l).

A.11 Ablation study on γ and t in CoCo-PnP

We report the PSNR values by CoCo-PnP with different γ and t in the deblurring task in Table 5. It can be seen that, the proposed methods are sensitive to γ , because it determines the denoising performance, but not sensitive to t.

A.12 Low-dose CT reconstruction

In order to further illustrate the effectiveness of the proposed methods, we consider the sparse-view low-dose CT reconstruction task. In this task, K=R is the Radon transform, and f in Eq. (1) is the down-sampled data in the Radon field. The Radon field data is corrupted by the Poisson noise.

⁵The data is kindly provided by [62] in github.com/photon-efficient-imaging/single-photon-camera.

Table 5: PSNR results by CoCo-PnP with different γ and t when deblurring the image '0005' from CBSD68 and kernel 8 from Levin's dataset. The Poisson noise level is 50. We run the algorithm for 500 iterations to ensure the convergence. When $\gamma=0.25,\,t_0(\gamma)=1/3,$ thus t<1/3. When $\gamma=0.5,\,t_0(\gamma)\approx0.3761,$ thus $t\leq0.3761.$

$\gamma = 0.25$	t	0.3333	0.300	0.200	0.100	0.001
CoCo-ADMM	PSNR	25.33	25.31	25.30	25.24	25.16
CoCo-PEGD	PSNR	25.32	25.30	25.27	25.22	24.98
$\gamma = 0.50$	t	0.3761	0.300	0.200	0.100	0.001
CoCo-ADMM	PSNR	24.88	24.87	24.79	24.64	24.47
CoCo-PEGD	PSNR	24.84	24.82	24.71	24.54	24.35

For the test set, we select ten typical images from "the NIH-AAPM-Mayo Clinic Low Dose CT Grand Challenge" [45], see Fig. 5.

For the comparison methods, we use: FBP, the conventional filtered back projection method; PWLS-TGV, penalized weighted least-squares (PWLS) with total generalized variation (TGV) prior [48]; PWLS-CSCGR, PWLS with convolutional sparse coding and gradient regularization [5]; UNet, which take the result by FBP as the input [31]; WNet, which uses two UNets to construct the data from both the image and Radon domain [14].

We show the reconstruction results with 60 projection views and Poisson noises with peak value p=100,500 in Table 2. It can be seen that, compared with two iterative PWLS-based methods, and two end-to-end deep learning methods, the proposed CoCo methods have a significant improvement in PSNR and SSIM values.

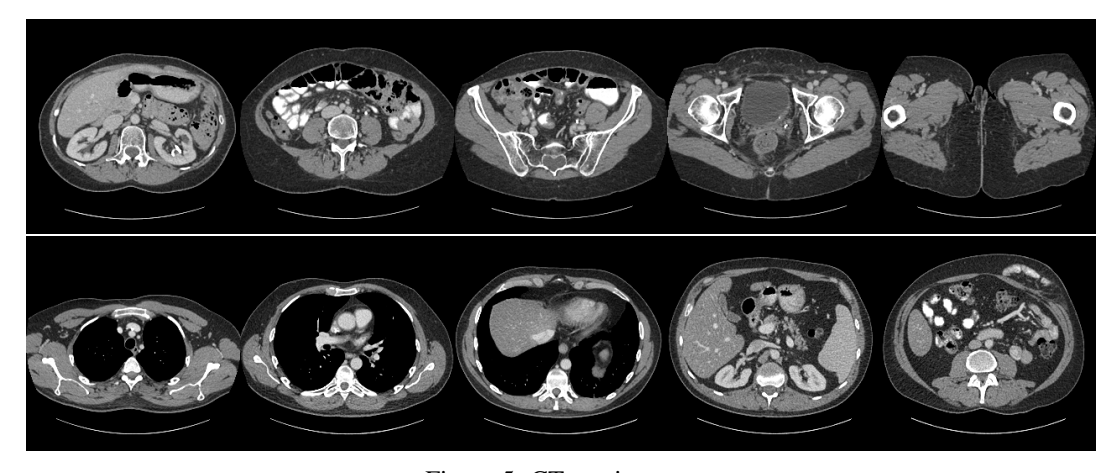


Figure 5: CT test images.

A.13 Poisson denoising results

We apply CoCo-ADMM and CoCo-PEGD to Poisson denoising problems. In this task, $K={\rm I}$ is the identity. The average PSNR and SSIM values on CBSD68 are summarized in Table 6. It can be seen that compared with other convergent methods, the proposed methods achieve the best PSNR and SSIM values. It validates the effectiveness of CoCo methods.

A.14 Computational cost

In Table 7, we give the average computation time in seconds, as well as the memory cost in MB by different methods when deblurring a 256×256 image. It can be seen that the proposed methods are the most efficient with least memory cost.

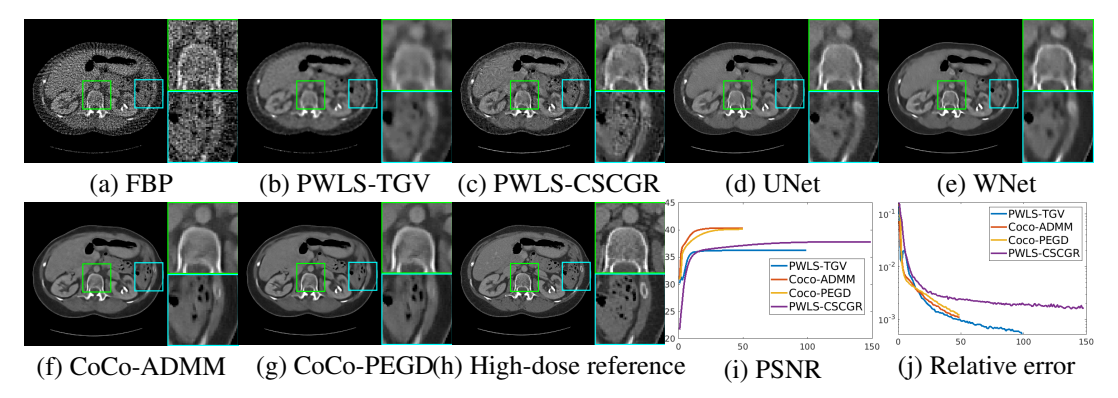


Figure 6: Sparse view CT reconstruction results with 60 views and Poisson noises (peak=500). (a) FBP, PSNR=30.91dB. (b) PWLS-TGV, PSNR=36.12dB. (c) PWLS-CSCGR, PSNR=37.80dB. (d) UNet, PSNR=38.54dB. (e) WNet, PSNR=38.74dB. (f) CoCo-ADMM, PSNR=40.46dB. (g) CoCo-PEGD, PSNR=40.28dB. (h) High-dose reference. (i) PSNR curves. (j) Relative error curves.

Table 6: Average denoising PSNR and SSIM performance by different methods on CBSD68 with peak value p=30 and p=20.

	p =	= 30	p = 20		
	PSNR	SSIM	PSNR	SSIM	
DPIR	29.85	0.8654	28.68	0.8300	
RMMO-DRS	27.90	0.8008	27.74	0.7887	
Prox-DRS	28.99	0.8087	27.94	0.7724	
SNORE	29.47	0.8474	28.34	0.8226	
PnPI-HQS	29.90	0.8613	28.63	0.8156	
B-RED	28.80	0.8041	26.26	0.7362	
CoCo-ADMM	29.99	0.8604	28.76	0.8329	
CoCo-PEGD	29.99	<u>0.8625</u>	28.77	$\overline{0.8332}$	

A.15 Performances under extreme conditions

In Fig. 7, we show an example when deblurring an image under severe noisy condition. It can be seen in Fig. 7 (a) that the image is severely corrupted. We compare results by different methods. It can be seen that CoCo-ADMM and CoCo-PEGD provide sharper edges. Even in this extreme case, the proposed methods are still convergent, see Figs. 7 (m)-(n).

A.16 Ablation study on the parameters α_1 and α_2

$$Loss(\theta) = \mathbb{E} \| D_{\sigma}(x + \xi; \theta) - x \|_{1} + \alpha_{1} \| J - J^{\top} \|_{*} + \alpha_{2} \max\{ \| 2\gamma J - I \|_{*}, 1 - \epsilon \}.$$
 (97)

In the loss function (97), α_1 controls the penalty strength of the Hamiltonian term to encourage conservativeness, and α_2 controls the penalty strength of the spectral term to encourage cocoerciveness.

As shown in Table 8, DRUNet without regularization terms has an expansive residual part. When α_1 gets bigger, the mean symmetry error gets lower. When α_2 is smaller than 1e-2, the regularized denoiser may not be cocoercive.

	B-RED	Prox-DRS	SNORE	DiffPIR	DPS	CoCo-ADMM	CoCo-PEGD
Iteration	300	100	200	100	1000	50	100
Time	42.5s	13.6s	74.1s	11.8s	177s	5.24s	9.08s
Memory	4946MB	3982MB	3624MB	2998MB	4694MB	2304MB	2304MB

Table 7: Average computation time in seconds, and memory cost in MB by different methods when deblurring a 256×256 image.

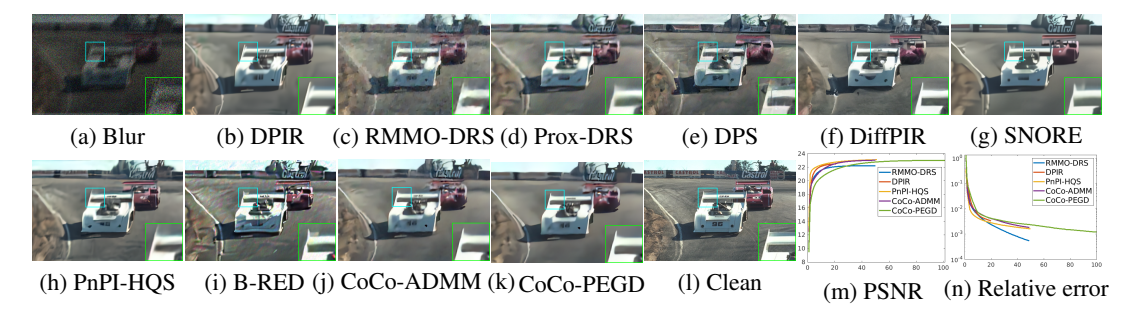


Figure 7: Deconvolution results by different methods on the image '0005' from CBSD68 with kernel 8 and p=10 Poisson noises. (a) Blur image. (b) DPIR, PSNR=22.49dB. (c) RMMO-DRS, PSNR=22.23dB. (d) Prox-DRS, PSNR=22.54dB. (e) DPS, PSNR=20.70dB. (f) Diff-PIR, PSNR=21.66dB. (g) SNORE, PSNR=23.31dB. (h) PnPI-HQS, PSNR=23.14dB. (i) B-RED, PSNR=21.15dB. (j) CoCo-ADMM, PSNR=23.04dB. (k) CoCo-PEGD, PSNR=23.02dB. (l) Clean image. (m) PSNR curves. (n) Relative error curves. x-axis denotes the iteration number.

Therefore, we set the penalty parameters large enough to encourage the properties we want. However, when α gets too large, the denoising performance may be sacrificed. We empirically set $\alpha_1=1$, $\alpha_2=1\text{e-}2$ in the experiments.

Table 8: Mean symmetry error $\|\mathbf{J} - \mathbf{J}^{\top}\|_{*}$ with N = 1 and maximal values of the norm $\|2\gamma \mathbf{J} - \mathbf{I}\|_{*}$ with N = 30 on CBSD68 for various noise levels σ and $\gamma = 0.50, 0.25$.

	15	25	40	Norms	α_1	α_2
DRUNet	4.1e+0	4.2e+1	1.8e+1	$\ \mathbf{J} - \mathbf{J}^{\top}\ _{*}$	0	0
$0.50 ext{-}CoCo ext{-}DRUNet$	8.6e-3	2.5e-4	7.1e-4	$\ \mathbf{J} - \mathbf{J}^{\top}\ _{*}$	1	1e-2
$0.50 ext{-}CoCo ext{-}DRUNet$	2.9e-1	2.6e-2	9.5e-2	$\ \mathbf{J} - \mathbf{J}^{\top}\ _{*}$	1e-2	1e-2
0.25-CoCo-DRUNet	3.1e-4	1.8e-4	3.9e-4	$\ \mathbf{J} - \mathbf{J}^{\top}\ _{*}$	1	1e-2
$0.25 ext{-}CoCo ext{-}DRUNet$	5.9e-1	8.5e-1	7.9e-1	$\parallel \mathbf{J} - \mathbf{J}^{\top} \parallel_{*}$	1e-2	1e-2
DRUNet	3.285	4.343	6.283	$\parallel \mathrm{J} - \mathrm{I} \parallel_*$	0	0
0.50-CoCo-DRUNet	0.994	0.992	0.972	$ J - I _*$	1	1e-2
0.50-CoCo-DRUNet	1.011	1.244	1.500	$\parallel \mathrm{J} - \mathrm{I} \parallel_*$	1	1e-3
0.25-CoCo-DRUNet	0.986	0.969	0.982	$\ 0.5 \mathrm{J} - 1\ _*$	1	1e-2
0.25-CoCo-DRUNet	0.992	1.010	1.211	$ 0.5\mathrm{J} - \mathrm{I} _*$	1	1e-3



Figure 8: Blind decovolution results by different methods.

A.17 Blind Deblur Results

In this section, we evaluate the performance of our proposed methods on real-world blind deblurring. We select 18 images from the dataset by Lai et al. [35], which captures challenging real-world blurry scenes. Four state-of-the-art methods are benchmarked: Deblur-INR [76], Lv et al. [42], DPIR [77], and RMMO [66]. Deblur-INR is a self-supervised method that jointly estimates clean images and blur kernels, while Lv et al. [42] applies total variation regularization to refine latent image estimation in a blind deblurring framework. In contrast, DPIR, RMMO, and our proposed CoCo-ADMM/CoCo-PEGD require pre-estimated blur kernels as input. To ensure fairness, all

	INR	Lv et al.	DPIR	RMMO	CoCo-ADMM	CoCo-PEGD
Average	0.2990	0.3444	0.3629	0.2664	0.5461	0.5474

Table 9: Average CLIP-IQA results across all deblurred images

kernel-dependent methods utilize blur kernels generated by the blind deblurring framework of Liu et al. [42]. Visual comparisons in Fig. 8 demonstrate that CoCo-ADMM and CoCo-PEGD produce sharper textures and fewer artifacts than baseline methods.

For quantitative evaluation, we employ the CLIP-IQA metric [70], a non-reference image quality assessment tool that leverages the pretrained vision-language representation of CLIP (Contrastive Language–Image Pretraining) to evaluate perceptual quality without requiring pristine reference images. The average CLIP-IQA scores across all deblurred images are summarized in Table 9. Despite relying on the same estimated kernels as DPIR and RMMO, our methods achieve superior performance, highlighting their robustness to kernel estimation errors and enhanced restoration capability.

A.18 Blind Denoise Results

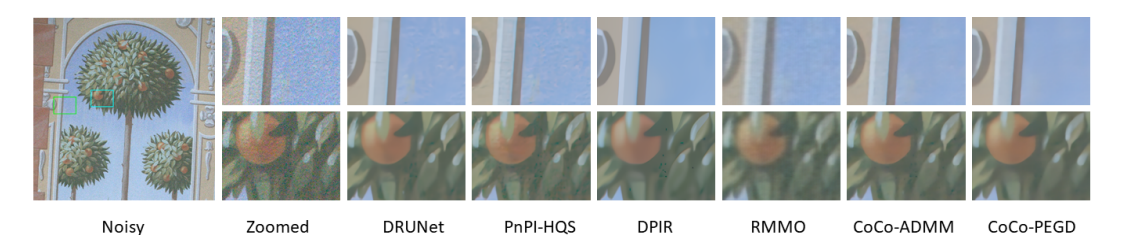


Figure 9: Blind noise removal results by different methods.

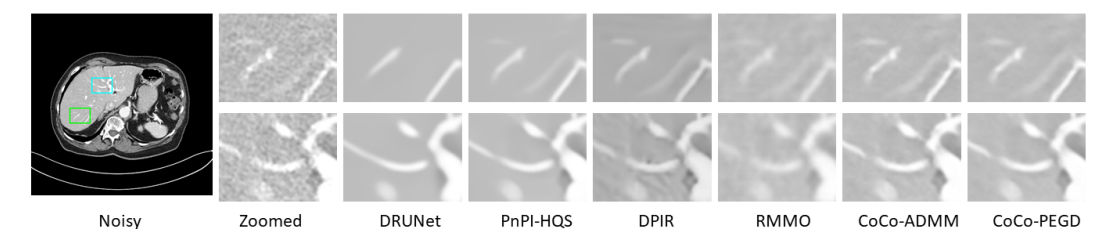


Figure 10: Blind noise suppression results in CT images by different methods.

In this section, we evaluate the performance of our proposed denoising framework on two benchmark datasets that capture real-world noise characteristics. For medical imaging, we employ the Low-Dose CT dataset from Mayo Clinic [46], which provides paired low-dose CT scans with Poisson noise.

For natural images, we utilize the DND dataset [52], comprising 50 real noisy photographs corrupted by a mixture of Poisson and Gaussian noise. Following the standard evaluation protocol, perceptual quality is quantified using the CLIP-IQA metric [70].

To ensure a fair comparison, we benchmark our proposed methods (CoCo-ADMM and CoCo-PEGD) against five representative techniques: DRUNet[77], DPIR [77], RMMO [66], and PnPI-HQS [71]. Quantitative results in Table 10 demonstrate that our proposed methods achieve state-of-the-art performance across both imaging domains.

	DRUNet	DPIR	RMMO	PnPI-HQS	CoCo-ADMM	CoCo-PEGD
Color images	0.4464	0.4509	0.4561	0.4586	0.4596	0.4593
CT	0.4154	0.4258	0.4398	0.4011	0.4707	0.4730

Table 10: Average CLIP-IQA results for blind image denoising.